Unclassified

DTIC FILE COPY

(2)

AD-A227 048

DTIC ELECTE SEP 25 1990 S B C8 D

DOCUMENTATION PAGE

Form Approved OMB No. 0704-0188

Unclassified

1b. RESTRICTIVE MARKINGS

2a. SECURITY CLASSIFICATION AUTHORITY

3. DISTRIBUTION/AVAILABILITY OF REPORT
Approved for public release; distribution is unlimited.

2b. DECLASSIFICATION/DOWNGRADING SCHEDULE

4. PERFORMING ORGANIZATION REPORT NUMBER(S)

5. MONITORING ORGANIZATION REPORT NUMBER(S)
AFOSR.TR.90-1026

6a. NAME OF PERFORMING ORGANIZATION
University of California

6b. OFFICE SYMBOL (If applicable)

7a. NAME OF MONITORING ORGANIZATION
AFOSR/NA

6c. ADDRESS (City, State, and ZIP Code)
Mechanical Engineering Dept.
Berkeley, CA 94720

7b. ADDRESS (City, State, and ZIP Code)
Building 410, Bolling AFB DC
20332-6448

8a. NAME OF FUNDING/SPONSORING ORGANIZATION
AFOSR/NA

8b. OFFICE SYMBOL (If applicable)
NA

9. PROCUREMENT INSTRUMENT IDENTIFICATION NUMBER
AFOSR 88-0011

8c. ADDRESS (City, State, and ZIP Code)
Building 410, Bolling AFB DC
20332-6448

10. SOURCE OF FUNDING NUMBERS

PROGRAM ELEMENT NO.	PROJECT NO.	TASK NO.	WORK UNIT ACCESSION NO.
61102F	2308	A2	

11. TITLE (Include Security Classification)
(U) Opposed Jet Turbulent Diffusion Flames

12. PERSONAL AUTHOR(S)
L. Talbot

13a. TYPE OF REPORT	13b. TIME COVERED	14. DATE OF REPORT (Year, Month, Day)	15. PAGE COUNT
Final	FROM 10/1/87 TO 3/31/90	September 5, 1990	68

16. SUPPLEMENTARY NOTATION

17. COSATI CODES			18. SUBJECT TERMS (Continue on reverse if necessary and identify by block number)
FIELD	GROUP	SUB-GROUP	Turbulent diffusion flames, Rayleigh scattering

19. ABSTRACT (Continue on reverse if necessary and identify by block number)

A Hydrogen-Helium mixture was chosen to investigate the structure of a counterflow diffusion flame. Reacting and non reacting conditions were studied at the same Reynolds number. To study the reaction zone structure, high speed tomography based on Mie scattering was employed using a copper vapor laser and a Fastax high speed camera. LDV measurements were also obtained. Different seeding techniques were used to visualize both the turbulent air and fuel jets. The tomographic records were digitized and recorded in a digital computer for statistical treatment. Significant differences in the wrinkle scales between the reacting and non reacting flows were found. A fractal statistical analysis of the tomography records was done to quantify these differences. Seeding of both fuel and air jets provided a mean for the evaluation of the reaction zone thickness. The strain of the reaction zone was obtained from the time resolved tomographic records. Local flame extinction and reignition were observed for different H2/Helium fuel mixtures.

• (continued on reverse side)

20. DISTRIBUTION/AVAILABILITY OF ABSTRACT
☒ UNCLASSIFIED/UNLIMITED ☐ SAME AS RPT. ☑ DTIC USERS

21. ABSTRACT SECURITY CLASSIFICATION
Unclassified

22a. NAME OF RESPONSIBLE INDIVIDUAL	22b. TELEPHONE (Include Area Code)	22c. OFFICE SYMBOL
Julian M Tishkoff	(202) 767-0465	AFOSR/NA

DD Form 1473, JUN 86 Previous editions are obsolete. SECURITY CLASSIFICATION OF THIS PAGE

Unclassified

19 (cont'd)

Historically, the evaluation of mixture fraction in combusting flow has required multiple concentration measurements. However, we have found it possible to choose a special fuel (85% He, 15% H2) which permits the measurement of the mixture fraction using only Rayleigh scattering. The Rayleigh intensity/mixture fraction correspondence was verified experimentally in a laminar coflow flame. The influences of strain rate and differential diffusion effects were investigated by comparing computed and measured profiles of a laminar counterflow diffusion flame. The results obtained from these comparisons were encouraging and suggest that the established Rayleigh/mixture fraction correspondence is valid under both turbulent mixing and laminar strained flamelet combustion regimes.

FINAL REPORT

AFOSR Grant 88-0011
Opposed Jet Turbulent Diffusion Flames
Principal Investigator: L. Talbot
University of California at Berkeley

Objective: The objective of this research program has been to investigate experimentally the dynamics and structure of opposed jet turbulent diffusion flames, where a jet of fuel is directed counter to an oncoming airstream. This configuration is of fundamental interest in exploring the effects of strain and heat release on the fluid mechanics of turbulent diffusion flames, and additionally exhibits some of the characteristics of boundary layer separation caused by transverse fuel injection in certain types of combustors.

Principal results: The majority of the experiments were carried out using a fuel jet composed of a mixture of hydrogen and helium, whose composition could be varied, while maintaining essentially constant jet Reynolds number, to explore the effects of burning rate and heat release on the flame structure.

The experimental techniques employed included high speed laser tomography using a copper vapor laser synchronized with a Fastax camera with silicone oil aerosol and titanium dioxide particles as the scattering media, laser velocimetry, and Rayleigh scattering. The scattering media permitted the imaging separately of the fuel stream, the airstream and the two in combination. Fractal analysis was performed on the flame interface, to determine its length scales, and individual flame structures could be identified and followed in time to determine the local stretch rate of the flame interface. Joint pdf's of axial and transverse velocity components were constructed which provided information on entrainment rates.

The fractal analysis revealed that the smallest scales or wrinkle dimensions of the flame front are increased by heat release, as are the largest scales. In the stagnation region of the flame, the flame front thickness is comparable to that of a laminar diffusion flame and correlates well with the length scale associated with the local strain rate, which is largest in the stagnation region. In contrast, the entrainment rate away from the stagnation region correlates with the largest scales associated with the vortex structure of the shear layer. The strain rate, which is highest in the stagnation zone, increases with heat release and a correlation exists between strain rate fluctuations and fluctuations in reaction zone position.

At the lowest concentrations of hydrogen in the hydrogen-helium fuel mixture it was possible to produce local extinction at the stagnation point of the flame, even though combustion was maintained in the shear layer downstream of the stagnation zone. This was even more dramatically exhibited in the case of methane-air flames which have a lower extinction strain rate, and for which a large non-reacting "hole" in the flame was produced at high strains. It is evident that the opposed jet turbulent diffusion flame is an excellent configuration for the investigation of strain-induced extinction phenomena.

Parallel with our study of the opposed jet flame, we investigated the possibility that a particular fuel could be identified such that its Rayleigh scattering cross-section was an unique monotonic function of mixture fraction. We found that a 15% hydrogen - 85% helium fuel mixture meets this criterion and we demonstrated by means of measurements in a laminar opposed jet (Tsugi) flame that calculated and measured mixture fractions were in excellent

agreement. This opens up wide possibilities for mixture fraction related measurements in turbulent diffusion flames using this fuel.

Personnel.

In addition to the Principal Investigator, the following personnel were involved in the program.

Dr. Philippe J. Goix - postdoctoral researcher
Mr. Keith R. Leonard - graduate student
Dr. Robert K. Cheng - Lawrence Berkeley Laboratory staff scientist
Dr. Ian G. Shepherd - Lawrence Berkeley Laboratory staff scientist

Publications and Presentations

Two papers, based on the work described, are being prepared for publication. They are:

"Experimental Study of Turbulent Counterflow Diffusion Flame Structure", by P.J. Goix, K.R. Leonard and L. Talbot.

"Direct Measurement and Mixture Fraction in Reacting Flow Using Rayleigh Scattering", by P.J. Goix, K.R. Leonard, L. Talbot and J.Y. Chen.

Additionally, an invited presentation of earlier flame-stabilization work was given at the ICASE Workshop on Turbulent Combustion, October 1989, the proceedings of which will be published by Springer-Verlag:

"Flameholding in Unconfined Turbulent Premixed Flames", by I.G. Shepherd, J.R. Hertzberg and L. Talbot.

Poster presentations of the work on counterflow turbulent diffusion flames and mixture fraction measurements were given at the recent 23rd Symposium (International) on Combustion in Orleans, France, August 1990.

Preprints of the above mentioned papers and abstracts of the poster presentation are attached.

Significant Technical Interactions

Collaborations with Drs. J.Y. Chen and R. Dibble of the Sandia Combustion Research Facility were established and are still maintained. Significant technical interactions with Professor R. Bilger of the University of Sydney occurred during his semester-long visit at Berkeley. We also participated by invitation in the ICASE Combustion Workshop.

Inventions

None.

Experimental Study of Turbulent Counterflow Diffusion Flame Structure

P.J. Goix, K.R. Leonard and L. Talbot

Mechanical Engineering Department,
U.C. Berkeley, CA 94720.

ABSTRACT

Laminar counterflow combustion configurations have been studied extensively for the investigation of fundamental combustion phenomena, such as fuel dilution, strain rate, and pressure dependences on flame extinction limits. However very few studies have been performed on turbulent counterflow diffusion flames. The turbulent opposed flow configuration chosen here consists of a fuel jet pipe of d=6.4mm in diameter directed downward toward an air jet 50 mm in diameter, shielded with a concentric air jet of 130mm diameter. The vertical distance between the fuel jet exit and the air flow can be adjusted to investigate the influence of the overall strain rate along the centerline of this configuration. A Hydrogen-Helium mixture has been chosen to investigate the dilution effects on the structure of the diffusion flame. To investigate the combustion effects on the turbulent mixing, reacting and non reacting conditions have been studied at the same Reynolds number. In order to study the reaction zone structure, high speed tomography based on Mie scattering has been employed using a copper vapor laser and a Fastax high speed camera. Different seeding techniques have been used to visualize both the turbulent air and fuel jets. The tomographic records were digitized and recorded in a digital computer for statistical treatment. Significant differences in the wrinkle scales between the reacting and the non reacting flows were found. A fractal statistical analysis of the tomography records has been done to quantify these differences. Seeding of both fuel and air jets provided a mean for the evaluation of the reaction zone thickness. From the time resolved tomographic records an evaluation of the stretch of the reaction zone boundaries has been performed.

INTRODUCTION

An opposed jet turbulent diffusion flame is an interesting combustion configuration for several reasons. One is that it facilitates the study of the effect of strain on the reaction zone in the stagnation region and thus extinction phenomena can be readily investigated even under conditions when co-flowing turbulent diffusion flames may be unstable. A second interesting feature of this configuration is that it incorporates at least qualitatively some of the characteristics of the shock wave induced boundary layer separation which occurs ahead of transversally injected fuel jets such as those which have been considered for employment in scramjet combustors and indeed, the opposed jet configuration has itself been mentioned as a possible candidate for scramjet fuel injection although there are obvious drag penalties involved. Additionally, the configuration provides a challenging problem in the evolution of a combustion zone from a turbulent stagnation combustion zone to an entrainement controlled shear layer region. Laminar one-dimensional stagnation diffusion flames have been studied theoretically and experimentally quite extensively recently [1-3]. In particular the dilution effect and strain effect on the heat release variations and extinction limit conditions have been emphasized [2-3]. However very few studies have been done on such flames in turbulent flow conditions. How the turbulent strain rate a_t, and the bulk strain rate a_b, can affect the reaction zone structure of the flames is not well known, and the effect of turbulence on the mixing

process in a stagnation flame, is still an important issue.

Our purpose is to address this problem by studying experimentally a two opposed jets configuration in reacting and non-reacting conditions. In order to analyze the two boundaries of the reaction zone a high speed tomography laser diagnostic has been used to investigate an hydrogen/air turbulent diffusion flame. As hydrogen flame burns very fast, helium dilution has been used to slow down the chemistry. The advantages of choosing He for dilution are first to minimize the preferential diffusion effect between the hydrogen and the diluent and second to keep the dynamic flow field conditions as constant as possible when helium dilution effects are to be studied, Reynolds number effects and momentum fluxes remaining basically constant for different H2/He mixtures at constant mass flow rates. In order to investigate the dynamics of such a turbulent flowfield two component LDV measurements were carried out in reacting and non-reacting conditions for the same Reynolds number.

EXPERIMENTAL DETAILS

The Opposed Jet Burner

The combustion configuration investigated consisted of a fuel jet pipe of d=6.4mm diameter directed downward toward an air jet of 50mm, shielded by 130mm air jet coflow. In order to prevent preheating of the fuel at the jet exit, a small diameter cooling coil (d=2mm) was wrapped around the fuel pipe and, the whole fuel pipe was shielded with a ceramic tube. The air jet and the air coflow velocities have been matched at 5 m/s. Turbulence (u'/U= 8%) in the air flow was generated by a perforated plate. The vertical distance between the fuel jet exit and the air flow could be adjusted to vary the overall strain rate in the reaction zone. Hydrogen fuel with various levels of helium concentration were used to study the effect of dilution on the extinction of the counterflow diffusion flame. To investigate the structure and the dynamics of the flame, high speed tomography and laser Doppler velocimetry were used and will be described in the following section.

High Speed Laser Tomography

The laser tomography technique is based on Mie scattering and has been used extensively over the last ten years [4-8]. A laser light sheet of 60mm width and .5mm thickness is produced by a copper vapor laser and two cylindrical lenses as shown as Fig (1). The copper vapor laser provides 5 mJ pulses of 20ns duration at adjustable repetition rates up to 6khz at λ=511nm. To follow the high repetition rate of the laser we used a high speed Fastax camera to image the laser sheet. The Fastax image synchronization pulses are used to trigger the laser. The laser is fired every two camera pulses, to record the radiation illumination background coming from the flame. The film used to record the tomography events was Kodak 4X reversal (400 ASA). Two types of seeding particle were used, titanium dioxide (TiO2) and silicone oil particles. Titanium dioxide particles were produced by the reaction TiCl4 + 2H2O --> TiO2 + 4(HCl). By seeding the fuel jet with TiCl4 and H2O a very dense cloud of TiO2 can be obtained. This technique has been used by various authors. Zur Loye and Bracco [7], investigated the effects of the presence TiO2 and HCl on the combustion process and found it to be negligible. Silicone oil and (TiCl4 + H2O) were injected respectively in the air stream and the fuel stream using an atomizer through a bypass circuit. To determine at which temperature the maximum Mie scattering gradient corresponds for each type of particles, a cylindrical laminar diffusion flame burner was set up. The fuel and the air jets were seeded respectively with TiO2 and silicon oil and a Mie scattering point experiment similar to Kennedy and Kent [9] was carried out. Point temperature and Mie scattering measurements were recorded at the same locations using a Pt/Pt10%Rh thermocouple of 300 μm bead mean diameter. Fig(2) shows the comparison of the two normalized Mie scattering profiles and the temperature profile taken at 10mm from the burner exit. One can note the very sharp intensity decrease within the laminar reaction zone, since for tomography visualization our concern is the maximum intensity gradient. The temperatures corresponding to this criterion for both particle types are found to be 480K for the silicone oil and 420K for TiO2. A high speed tomography negative film frame is projected and is imaged by a video camera. The video signal is digitized and stored on a 512X512 I2S matrix memory with 256 grey levels. The scaling factors in the X and Y directions are .125 mm per pixel and and .105 mm per pixel respectively. After background removal a threshold corresponding to the maximum intensity gradient is determined from the grey level probability density function and the edge corresponding to this threshold is computed and stored for further statistical treatment.

Velocity Measurements

To measure the average flow field of the turbulent counterflow H2-diluted Helium/Air flame two component LDV point measurements were performed. Details of the two LDV components and the data acquisition are included in Cheng [9]. A Spectra-Physics 4 watt argon-ion laser was the light source for the two component (488nm and 514nm) LDA system which uses two TSI model 1980A frequency counters. Aluminium dioxide particles of .3 μm in diameter were chosen to track both the fuel and the air jets. Since the dynamic range of the velocity field in the counterflow diffusion flame was expected to be between 60m/s and 0 for the fuel jet region and in between 0 and 12m/s in the product and cold air region a differential frequency shifting of 5 Mhz for both components was chosen. To reduce the velocity signal frequency and the shifting requirements the two LDV channel's optics set up were rotated 45 degrees from the burner axis. The two velocity components were recored simultaneously and transformed to the original burner frame of reference for further statistics. The number of samples for each records was 8192.

RESULTS

The Two Opposed Jet Velocity Field

The turbulent counterflow configuration was studied under non reacting and reacting conditions. In both cases the fuel jet and air jet exits was separated by 190mm. The hydrogen fuel jet was diluted with 60% of Helium in volume. The Reynolds numbers based on the maximum jet velocities were 2700 and 3300 respectively for the non-reacting (N.R.) and reacting (R.) flow field. Figs 3 a ,b represent the average velocity vector fields of the turbulent opposed jets configurations in non-reacting and reacting conditions. In these figures the the velocity vectors are plotted in the X,Y plane where the jet centerline corresponds to Y=0, and X=0 corresponds to the fuel jet exit. In both cases the velocity field is axisymetric. One can note the difference in the penetration depth of the fuel jet between the N.R (Xp=45mm) and the R. (Xp=110mm) cases. The divergence of the flow field near the stagnation region is much stronger in combustion. These differences in penetration depths and divergence are mainly associated with volumetric expansion occuring during combustion. It is also clear from these two figures that the air flow streamlines diverge near the stagnation region and then rotate as they are entrained in large scale structures by the fuel jet. The size of these large scale structures differ from the R. to the N.R cases, being approximatively 40mm and 20mm respectively. In Figs (4 a,b) are plotted the centerline velocity profiles in both cases. In both cases the fuel and the air jets have been seeded separately with Al2O3 particles. One can note significant differences between the two cases even though both the air jet exit and the fuel jet exit velocities are matched to +5m/s and -65m/s respectively. The average strain rates deduced from these profiles at different jet locations are given in Table 1. At the stagnation region the average strain rate values are found to be $800s^{-1}$ (fuel side) and $55s^{-1}$ (air side) for the N.R case and 500 s^{-1} reacting (fuel side) and $95s^{-1}$ (air side). In order to have a better understanding of the flow field, joint probability density functions of the two velocity components have been computed in both the shear and stagnation region in reacting conditions. In each case the fuel and the air jets have been seeded separately. Figs 5 a,b represent joint pdf contours, jpdf(u,v) computed at the stagnation region. These contours correspond to 70%, 40% and 20% of the maximum peak value. For each case Umean and Vmean axes are plotted. A comparison of Fig 5a and 5b show a clear bimodal behavior around the zero velocity due to the intermittency of the stagnation region. Since the velocity gradient is much steeper in the fuel side, the jpdf is much broader. Due to the intermittency even stationary particles in the stagnation region can give positive or negative velocity values, and one has to be careful in the determination of the average strain rate at the stagnation region. Figs 6 a-e and Figs 7 a-e represent the jpdf(u,v) contours measured and computed in the shear region where the combustion is taking place at -90mm and -100mm of the fuel jet exit (left side only, negative Y). The positions at which the jpdf(u,v) have been calculated are indicated on the velocity plots with a circle (Fig 3.a). The negative and positive transverse velocities point toward the outside and inside the fuel jet respectively as shown on Fig 8 where the four quadrants and their meanings are designated. In each case the Umean and Vmean axes are plotted. Figs 6 a-e indicate that both fuel and air fluid are rotated from quadrant 1 to quadrant 2, from X=-90m Y=-15mm to X=-90mm Y=-9mm, entraining hot products in the fuel side. Figs 7 a-e represent the same jpdf(u,v) for the same Y locations but in this case at X=-100mm. The joint pdf velocity contours are narrower particularly for the air seeded cases, and the rotation phenomenon pointed out previously is less pronounced. However we can still observe a 20% peak contour in the negative

longitudinal velocity quadrant, Fig 7 (a), indicating the beginning of the rotation from quadrant1 to quadrant2 representative of entrainment.

Tomography Results

Figs 9 a,b show instantaneous tomography snapshots, where the fuel only has been seeded with TiO2 particles. In both cases the images are bimodal in grey levels and the transition between the black region (air) and the bright one (fuel) is very sharp. In the cold condition this transition corresponds to the fuel/air jet interface and in combustion this interface is assumed to be an isotherm interface at Ti=420K as shown in Fig 2. These interfaces have been recorded in a PDP11 computer memory using a threshold continuity algorithm. In order to understand the wrinkle process of the highly convoluted interfaces, a fractal algorithm has been applied to the tomographic records. Fractal analysis has been recently used in turbulent combustion [11-15]. It has been shown by Mandelbrot [11] that a highly convoluted fractal surface can be described by three parameters which are the fractal dimension D, the inner cutoff ϵ_i and the outer cutoff ϵ_o. These three parameters can be interpreted respectively as the wrinkle scale hierarchy of the surface, the smallest wrinkle scale and the largest wrinkle scale of the surface. The fractal algorithm used here is a counter segment algorithm. This algorithm is similar to those used by Mandelbrot [11] and Gouldin et al [12] to analyze flame fronts in premixed combustion and is described in [13]. Basically the length of the digitized curve, representing either an isotherm or the fuel/air jet interface, is measured with a straight line segment ϵ which varies in size. The length $L(\epsilon)$ is obtained by the relationship $L(\epsilon)=N(\epsilon)\epsilon$ To minimize noise problems statistics over 30 samples have been processed. Figs 10 a,b show a comparison of the fractal plots corresponding to the typical tomography contours shown Figs 9 a,b. Both of the plots exhibit a fractal character, the evolution of the length versus the line segment size in log-log space is linear in both cases and the fractal dimension is found to be equal to D=2.18 (+/-.005) for the N.R. case and D=2.07 (+/-.005) for the R. case. The plots are linear for at least one decade of the log space. The inner cutoff and the outer cutoff are determined where the curves depart respectively at small and large ϵ from the fractal slope. For the N.R. case ϵ_i = 1.3mm and ϵ_o = 16mm while for the R. case ϵ_i = 2mm and ϵ_o = 20 mm. One can note *significant differences between the* N.R and the R. stagnation regions. Overall the fractal dimension is found to be much smaller in the reacting case, indicating a smoothing effect on the isotherms of the flow field due to the combustion. Another interesting feature to note is that both the inner cutoff and the outer cutoff in the reacting flow are larger than the non reacting case which indicates that the turbulent velocity spectra in combustion are shifted toward larger scales.

Figs 11 a,b represent two instantaneous tomography snapshots In this case both the fuel and air jets have been seeded with TiO2 and silicone oil particles. The reaction zone (black region) is clearly delineated by the two isotherms T_{tio2}, T_{oil}. The determination of the position of these two isotherm contours leads to a spatial determination of the reaction zone thickness. Qualitatively, the tomography pictures show a significant increase of the reaction thickness from the stagnation region toward the shear region. One can also see the vortex development along the shear region and entrainment of hot product gas in the fuel jet. From time sequences typical of Fig 11 a,b it is possible to isolate a turbulent structure in both the shear and stagnation regions and to determine their length evolutions with time. However the criterion chosen to isolate a turbulent structure is subjective, and we decided to isolate a turbulent structure when it is bound by a singularity (second derivative discontinuity) at each end. Following the singularities, we are then able to measure their lengths. This leads to a one dimensional evalution of the stretch factor $Str_1=1/L(t) * dL(t)/dt$, and assuming isotropic stretching of the surface area the stretch factor can be written as $Str_2=1/A(t) * dA(t)/dt=2 * Str_1$. The results obtained from the high speed tomography pictures for the stagnation region and the shear zone will be presented separately.

Stagnation Zone

The determination of stretch and the instantaneous laminar reaction zone thickness evaluation is very interactive and quite laborious, and for this reason at present statistics of those quantities over only 30 independent samples are presented. One sample correspond to two snapshots .57ms apart. The average turbulent reaction zone thickness is found to be $\epsilon_{rz}=1.5mm$ with an rms of .5 mm. The average stretch rate Str_2 deduced is equal to $1500s^{-1}$ with an rms of 650 s^{-1}. This rms could probabily be reduced by increasing the number of samples in the statistics. For comparison, the stretch rate has been also computed

at the stagnation region, for the same number of samples,in the non reacting flow case (N.R). The average stretch rate value obtained in the non reacting case is $Str_2 = 820\ s^{-1}$ with an rms of $450\ s^{-1}$. This value is significantly lower than the stretch rate in the N.R conditions. These differences will be discussed later. It is however worth noting that the strain rate determination requires a highly convoluted contour (representing the highest strain rate) and the statistical evaluation of the stretch may correspond to the upper bound of the turbulent stretch distribution. Fig 12 a represents the pdf of the position of the lean side reaction zone (air boundary), marked by the isotherm T_{oil}=480K. This pdf has been obtained from 200 time-independent samples along the centerline. From this pdf the rms of the reaction zone position in the stagnation zone is determined to be 3.5 mm.

Recirculation Zone

Fig 12 b represents the evolution of the pdf of position of Ti_{oil}, along the shear layer. The rms of position deduced from the pdf decreases from 3.25 mm at X= -100 mm to 2.5 mm at X= -95 mm and is constant up to X= -75 mm. These results indicate the stabilizing role played by the recirculation region in opposing the jet's lateral movements. As has been done for the stagnation region, the stretch factor has also been determined along the shear layer. It is clear Fig 11 b that while the shear turbulent structures are being rolled up they are convected downstream. The stretch factor during the roll up varies between 100 s^{-1} and 800 s^{-1} while the convection speed of the structure varies between 6 m/s and 13 m/s where the velocity vector always diverges from the axis of symmetry.

DISCUSSION

The mixture fraction variable, Z, a conserved scalar, is very useful in the modeling of the internal structure of diffusion flames [16-18]. By definition, the mixture fraction is bounded by 0 in pure oxidant and by 1 in pure fuel. Assuming fast chemistry and thermodynamic equilibrum, the temperature of the flame in mixture fraction space can be obtained. Fig 12 shows the temperature profile in mixture fraction space for the conditions of the H2-helium/air diffusion flame studied. The temperature and mixture fraction at the stoichiometric surface are T=2000 K and $Z_s = 0.1$ respectively. The problem is to find the correspondance between the mixture fraction and physical space. As shown by Bilger [16], Peters [17] and Williams [18] , using the fuel and oxidant mass fraction conservation equations one can derive an equation for the mixture fraction under a constant diffusivity approximation,

$$\rho\frac{\partial Z}{\partial t} + \rho v\nabla Z = \nabla(\rho D\nabla Z) \tag{1}$$

For a laboratory coordinate system in the case of a steady laminar stagnation flame this equation can be written as follows:

$$\rho u\frac{\partial Z}{\partial x} = -\frac{\partial}{\partial x}(\rho D\frac{\partial Z}{\partial x}) \tag{2}$$

Assuming ρD constant and a constant strain rate a_s one can obtain an analytical solution for the mixture fraction:

$$Z(x) = \frac{erfc(sx^2)}{2} \tag{3}$$

where: $s = \frac{a_s}{2D}$, $\frac{1}{\sqrt{s}}$ has a length scale dimension which can be related to the reaction zone thickness of the laminar diffusion flame. Our purpose here is to compare the instantaneous thickness of the reaction zone of the turbulent opposed jet diffusion flame determined by high speed tomography, with the thickness calculated for the laminar case under the same strain rate conditions. The comparison shown in Fig 2 of the maximum intensity gradient with a temperature profile in a laminar case for Tio2 and oil particles provides a means of marking the isomixture fraction values Z_{tio2} and Z_{oil}. Using the temperature/mixture fraction plot of Fig 13 as a look up table, we can evaluate the isomixture fraction contours corresponding to the oil and TIO2 maximum intensity gradient contours, which are Z_{oil} = .001 and Z_{Tio2} = .8. Several experimental and theoretical studies of laminar opposed jet reacting flows have shown that the laminar velocity profile in the reaction zone is not monotonic. In particular, Tsuji [1] and more recently Pellet et al [3] have shown that the typical velocity profile increases linearly, crossing the stagnation region, from the

jet side to the flame (the stochiometric mixture fraction) and then decreases sharply in a region called the "upstream boundary of flame front" and finally increases linearly on the air jet side. In all cases the velocity gradients on the air side are much smaller than the gradients on the fuel side. The sharp gradient between the flame and its upstream boundary position is attributed to the heat release and usually occurs in a very thin region typically 0.2 mm in width. In our case this sharp gradient must occur between Z_s=.1 and Z=0. It was not possible to resolve this region with our velocity measurements due to the intermittent movement of the reaction zone. However, as shown in Table 1 the gradients on the air side are about five time smaller than on the fuel side. Figs 14 a,b show the laminar reaction zone profiles deduced from equation (3). The diffusivity coefficient chosen is D (He-N2) at T=298 K and also at T=1150K which corresponds to (Tmax+ Tmin)/2. The strain rate has been varied from 500 s^{-1} to 1500 s^{-1} which are basically the average strain rate deduced from the average fuel centerline velocity profile and the stretch rates deduced from the tomography length measurements. The mixture fraction gradients deduced from these curves from Z_{tio2} = .8 to Z = .1 are given in Table 2 together with the average mixture fraction gradient obtained from the instantaneous tomography snapshots. From these comparisons, the curves obtained with D(He-N2) evaluated at Tmean=1150K seem to give results similar to those measured while D(He-N2) for 298K leads to a much steeper mixture fraction gradient. The best fit seems to be at a=1000 s^{-1} which is between the average strain rate 500 s^{-1} and the average stretch rate 1500 s^{-1}. It is worth noting that the rms of the reaction zone thickness is 0.5 mm and using the reaction thickness deduced from eq (3), this rms corresponds to a strain rate of 500 s^{-1}. Since the local stretch rate was deduced empirically (when the stagnation zone was sufficiently wrinkled) it might correspond to the smallest scales of the turbulence spectrum and thus to the maximum instantaneous strain rates. This suggests that the reaction zone fluctuations can be correlated to the strain rate fluctuations. A more consistent statistical analysis of both the reaction zone thickness and the instantaneous stretch rate is necessary to confirm this trend. The effect of nitrogen dilution on H2/air diffusion flame extinction was investigated by Dixon-Lewis and Missaghi [2]. They found in particular a significant decrease in peak temperature beginning for strain rates between 100 s^{-1} and 1000 s^{-1}, for an equimolar hydrogen/nitrogen mixture. In the case of the hydrogen/helium mixture investigated here no extinction has been observed. However, the pdf of reaction zone position presented in Fig 12, clearly shows two modes. Since we have seen that the average flow field in combustion exhibits a penetration depth which is twice the penetration depth under cold conditions, heat release might induce strong penetration depth fluctuation and might explain the two peaks in the reaction zone position pdf.

CONCLUSION

A turbulent opposed jet H2-He diffusion flame has been investigated experimentally by high speed tomography and two component laser velocimetry. Different seeding techniques have been used to visualize both sides of the reaction zone (fuel and air sides). A fuel mixture (60% He, 40% H2) at a Reynolds number close to 3000 has been investigated in both reacting and non-reacting conditions. From the velocity field measurements and the tomography visualizations two main regions have been identified:

- Shear region: where the hot product entrainment into the fuel jet is significant and occurs at large scales.
- Stagnation region: where the turbulence wrinkles the reaction zone and moves it back and forth around an average stagnation point location.

A fractal segment counting algorithm was applied to the tomography records and the smallest, largest and fractal dimensions of the wrinkle scales on the fuel side of the stagnation region have been deduced. A local stretch factor has also been estimated for non-reacting and reacting conditions. By simultaneous seeding of both fuel and air jets, the instantaneous reaction zone thickness was obtained and an average thickness and rms were deduced from a small number samples. From these results we have found:

1) The size of the wrinkles in the fuel jet stagnation zone are much larger in the reacting case than in the nonreacting case.

2) The instantaneous stretch rate is higher at the stagnation zone than in the shear zone.

3) Although the wrinkle scales are smaller in the non-reacting case, the stretch value is higher in the reacting case. This indicates a possible temperature induced viscosity increase effect on the wrinkling process.

4) The reaction zone thickness evaluated at the stagnation region scales with:

$$e_r = \sqrt{(\frac{2D}{a})}$$

where the coefficients are chosen as:

D, the He-N2 binary diffusion coefficient, evaluated at 1150K and

a, the strain rate, at 1000 s^{-1}.

This strain rate is midway between the average strain rate evaluated from the LDV measurements (500 s^{-1}) and the upper bound of the stretch evaluated from the tomographic time series (1500 s^{-1}). The rms of the reaction zone thickness seems to correspond to a strain rate rms of 500 s^{-1}. This result indicates a correlation between fluctuations of the reaction zone thickness and strain rate fluctuation. Further statistics are necessary to confirm this trend and are in progress.

AKNOWLEDGEMENT

The authors would like to express their appreciation to Dr. R.K. Cheng, Dr. I.G Shepherd and Mr. G.L. Hubbard from Lawrence Berkeley Laboratory for their assistance in the LDV setup, image processing software and useful discussions. This research was supported by the Air Force Office of Scientific Research under the Contract AFOSR-88-0011.

REFERENCES

(1) Tsuji, H., "Counterflow Diffusion Flames" *Progress Energy and Combustion Sciences*, vol. 8, pp93-119 1982.

(2) Dixon-Lewis, G.,Missaghi, M. "Structure and Extinction Limits of Counterflow Diffusion Flames of Hydrogen-Nitrogen Mixture in Air" 22snd Symposium Int on Combustion/The Combustion Institute 1988/pp 1461-1470.

(3) Drake, M. C., Blint, R.J., "Structure of Laminar Opposed-flow Diffusion Flames with CO/H2/N2 Fuel." *Combustion Sciences and Technology* vol. 61 pp 187-224 (1988)

(4) Boyer, L., "Laser Tomographic Method for Flame Front Movement Studies ", *Combustion and Flame*, vol. 39, no. 3, November 1980.

(5) Goix, P.J., Paranthoen, P., and Trinite, M., "A Tomographic Study of Measurements in a V-Shaped H_2/Air Flame and a Lagrangian Interpretation of the Turbulent Flame Brush Evolution", accepted to *Combustion and Flame*, 1989.

(6) Chew, T.C., Britter R.E., and Bray, K.N.C. "Laser Tomography of Turbulent Premixed Bunsen Flames", *Combustion and Flames*, vol 75, no. 2, February 1989.

(7) Zur Loye, A. O., Bracco, F. V., " Two-Dimensional Visualization of Premixed-Charge Flame Structure in an IC engine" International Congress and Exposition, Detroit Michigan February 23-27, 1987.

(8) Kennedy, I. M.,Kent, J.H., "Measurements of a Conserved Scalar in Turbulent Jet Diffusion Flames" Eightieth Symposium (Int) on Combustion pp 279-288 1980.

(9) Cheng, R. K., Talbot, L., Robben, F., "Conditional Velocity Statistics in Premixed CH4-Air and C2H4-Air Turbulent Flames" Twentieth Symposium (Int.) on Combustion/The Combustion Institute, 1984/pp. 453-461

(10) Gouldin, F.C., Hilton, S.M., and Lamb, T., "Experimental Evaluation of the Fractal Geometry of Flamelet", accepted at the 22nd session of the Combustion Institute, 1988.

(11) Mandelbrot, B.B., "Fractal Geometry of Nature", *W.H. Freeman and Company*, New York, 1983.

(12) Gouldin, F.C., "An Application of Fractals to Modeling Premixed Turbulent Flames", *Combustion and Flame*, vol. 68, no. 3, June 1987.

(13) Goix, P.J.,Shepherd, I.G., Trinite, M., "A Fractal Study of a Premixed V-Shaped H2/Air Flame" *Combustion Sciences and Technology*, vol. 63. pp. 275-286 1989.

(14) Sreenivasan, K.R. and Meneveau, C., "The Fractal Facets of Turbulence", *J.F.M.*, vol.17, pp.357-386, 1986.

(15) Sreenivasan, K.R., Prasad R.R, "Fractal dimension of scalar interfaces in turbulent jets", Polish Acad. Sci. vol 14, 1-14, 1988.

(16) Bilger, R., " Turbulent Diffusion Flame Structure", *Combustion Sciences and Technology* vol 13, no.1-6, 1976.

(17) Peters, N., "Laminar diffusion flamelet models in non premixed turbulent combustion" *Progress in Energy and Combustion Science* vol 10 no 3 1983.

(18) Williams, F.A., "Combustion Theory" 2nd Edition. The Benjamin-Cummings Publishing Company, Inc. 1985.

CAPTIONS

Fig 1 High speed laser tomography setup.

Fig 2 Comparison of the Mie scattering intensity profiles (TiO2 and silicone oil particles), with the temperature profile, obtained at 10 mm from the burner exit of a laminar diffusion flame.

Fig 3 Average velocity vector plots: (a) reacting conditions. (b) non-reacting conditions.

Fig 4 Centerline velocity profiles in both non-reacting conditions: (a) mean velocity U, (b) rms u'and v'.

Fig 5 Jpdf (u,v) contours obtained in reacting condition near the stagnation region of the two jets at 107 mm: (a) fuel jet is seeded, (b) air jet is seeded.

Fig 6 Jpdf (u,v) contours obtained in reacting condition in the shear region of the two jets at X= -90 mm for Y= -15 mm to -9 mm: (a), (c), (e) fuel jet seeded and (b), (d), (f) air jet seeded.

Fig 7 Jpdf (u,v) contours obtained in reacting condition in the shear region of the two jets at X= -100 mm for Y= -15 mm to -9 mm: (a), (c), (e) air jet seeded and (b), (d), (f) air seeded.

Fig 8 Schematic representing the four quadrants of the jpdf.

Fig 9 Instantaneous tomography snapshots of the two opposed jets. In both cases only the fuel is seeded with TiO2 particles: (a) non-reacting conditions (b) reacting conditions.

Fig 10 Typical fractal length plot in log-log space normalized by the outer cutoff length. (average of 30 samples): (a) non-reacting conditions, (b) reacting conditions.

Fig 11 Instantaneous tomography snapshots 570 μs apart. Fuel seeded with TiO2 and air seeded with silicone oil: (a) t=0, (b) t=570 μs.

Fig 12 Pdf of position of T=480K isotherm (air jet seeded with silicone oil) Reacting conditions. Statistics over 200 samples: (a) shear region, (b) stagnation region.

Fig 13 Reaction zone temperature profile in mixture fraction space.

Fig 14 Mixture fraction profiles near the stagnation zone using constant strain rate and constant diffusivity approximations. (a) D(He-N2) evaluated at 298K, (b) D(He-N2) evaluated at 850K.

TABLE I Average Strain Rates

	Re	$a_{air}[s^{-1}]$	$a_{fuel}[s^{-1}]$	$Str_2[s^{-1}]$
N.R.	2700	55	800	800
R.	3300	95	500	1500

TABLE II Mixture Fraction Gradients

	$a=1500s^{-1}$	$a=1000s^{-1}$	$a=500s^{-1}$	**Measured**
$\frac{\partial Z}{\partial x}$ (m-1)	350	475	630	530

SCHEMATIC

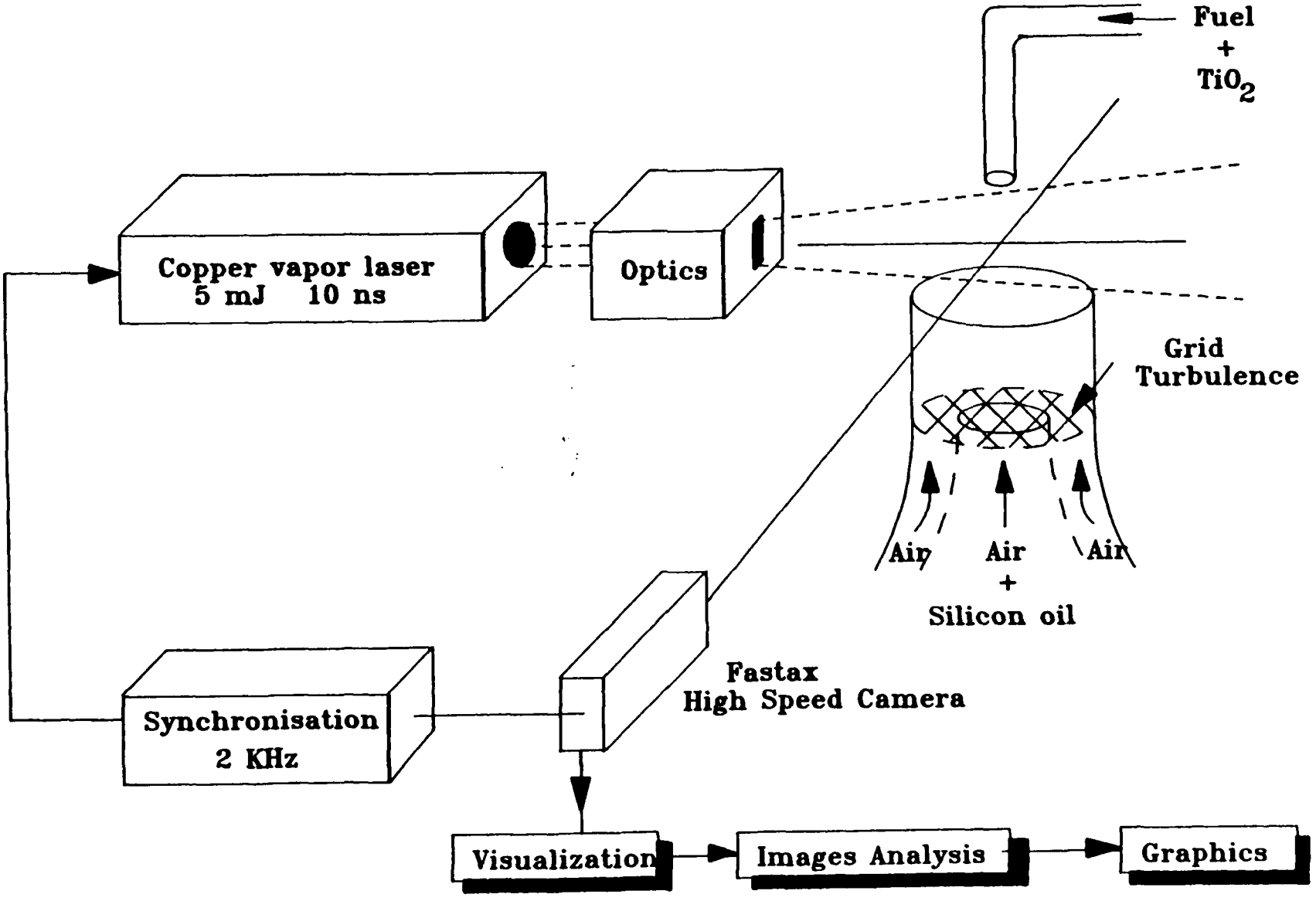

Fig 1

TEMPERATURE AND MIE SCATTERING INTENSITY PROFILES

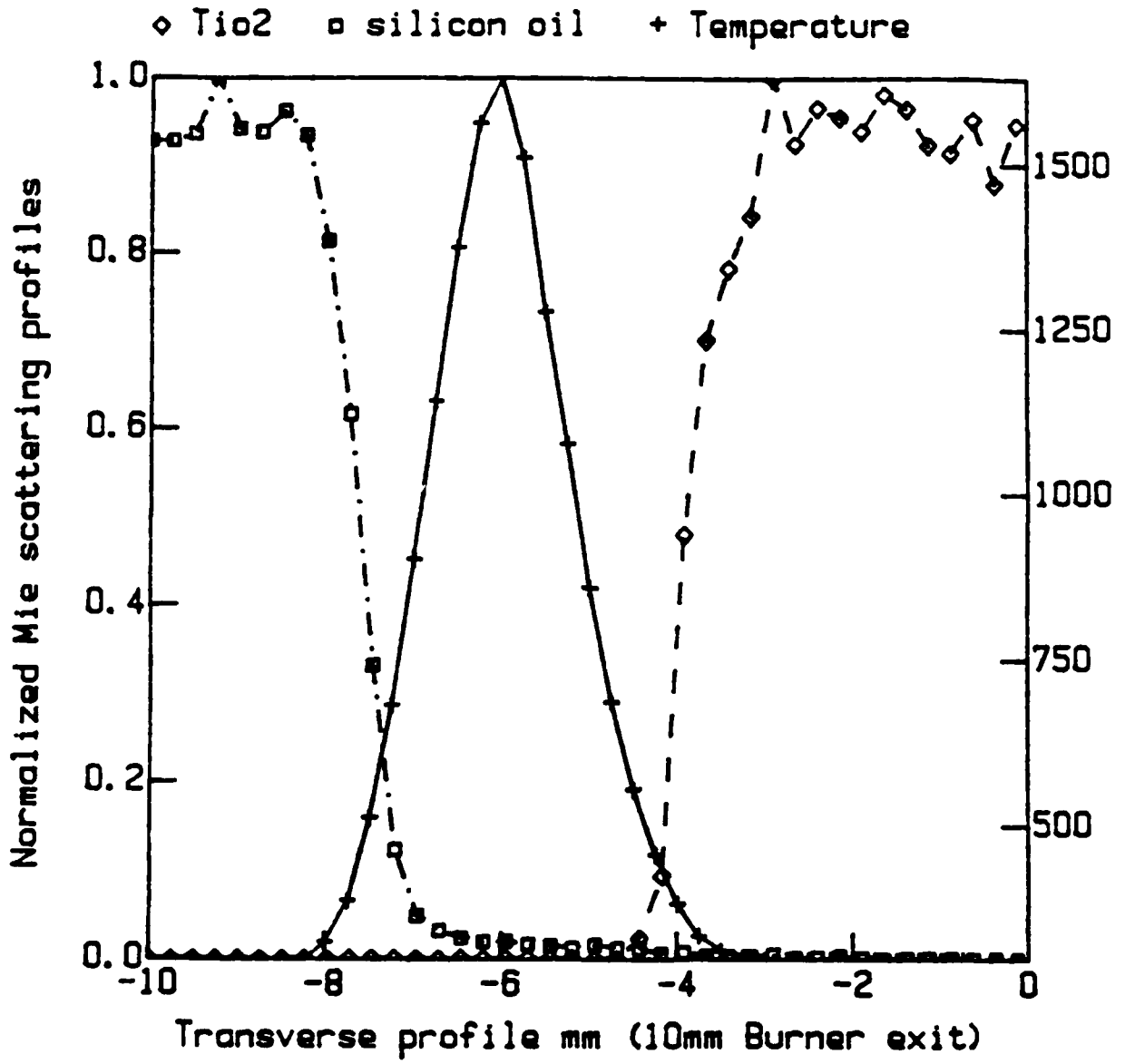

Fig 2

AVERAGE VELOCITY VECTOR FIELD

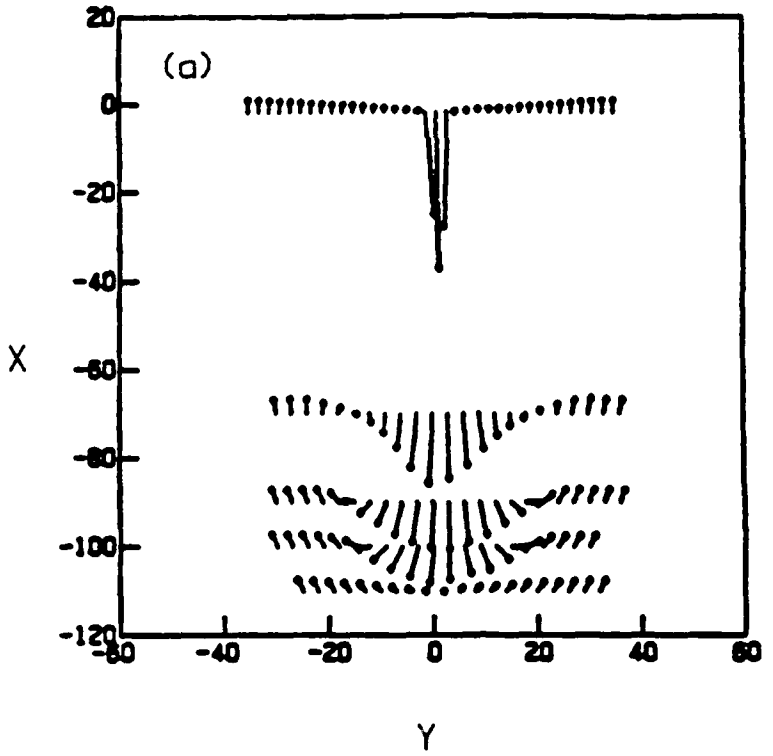

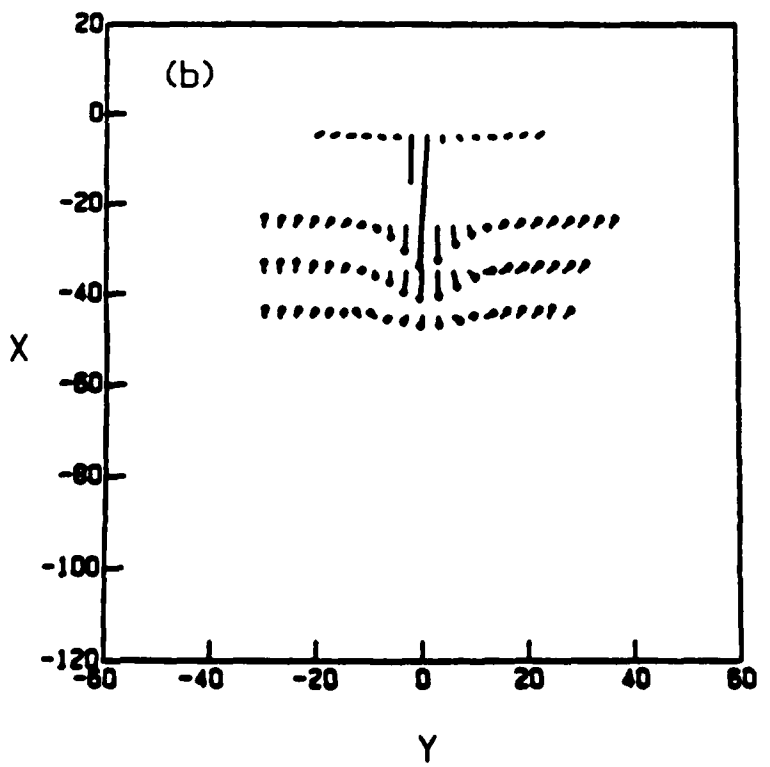

Fig 3

VELOCITY PROFILE ALONG THE CENTERLINE

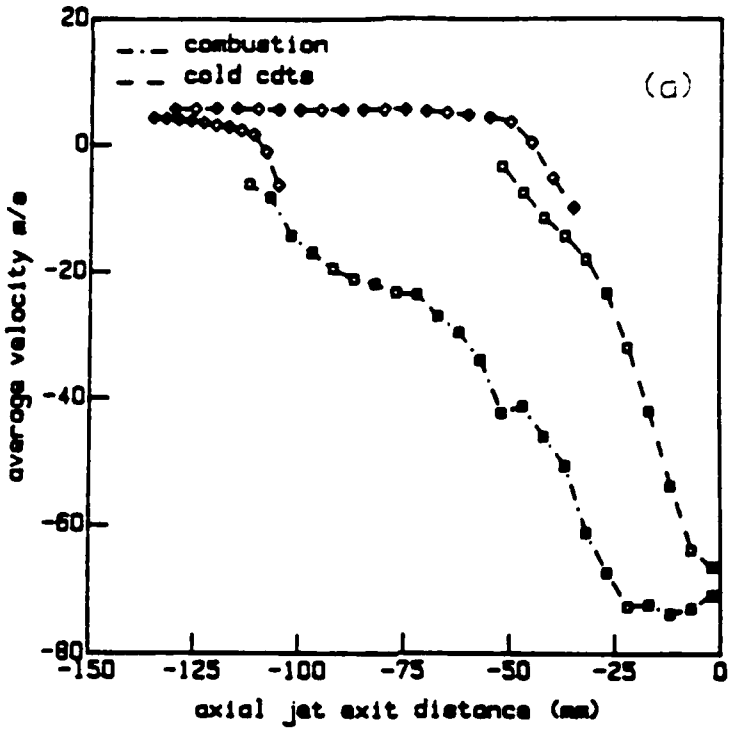

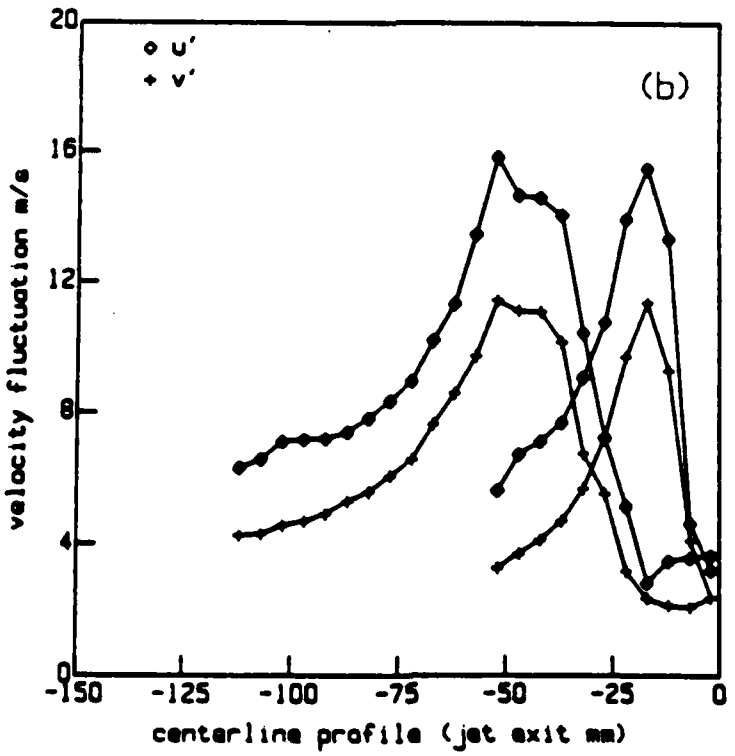

Fig 4

JPD(U, V) AT X=-110mm Y=0

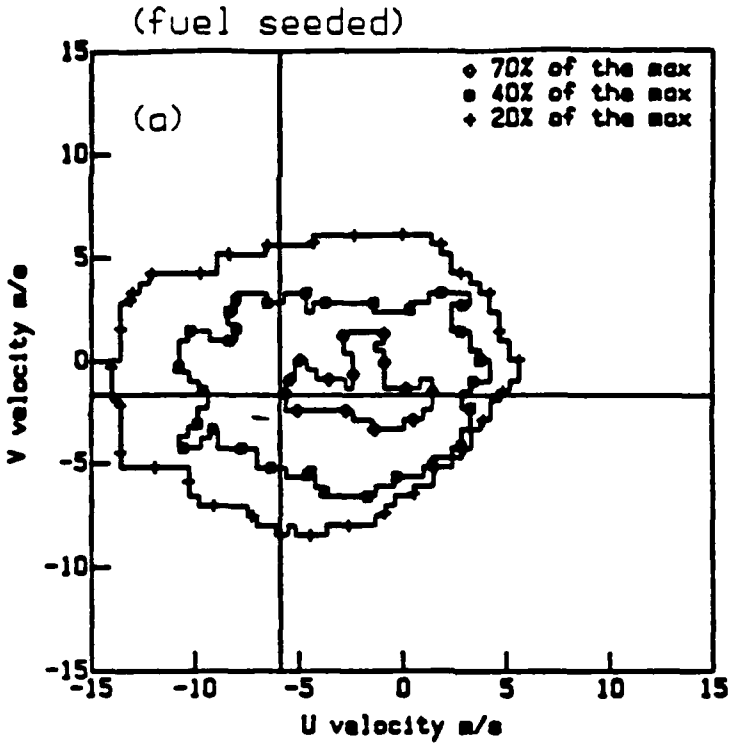

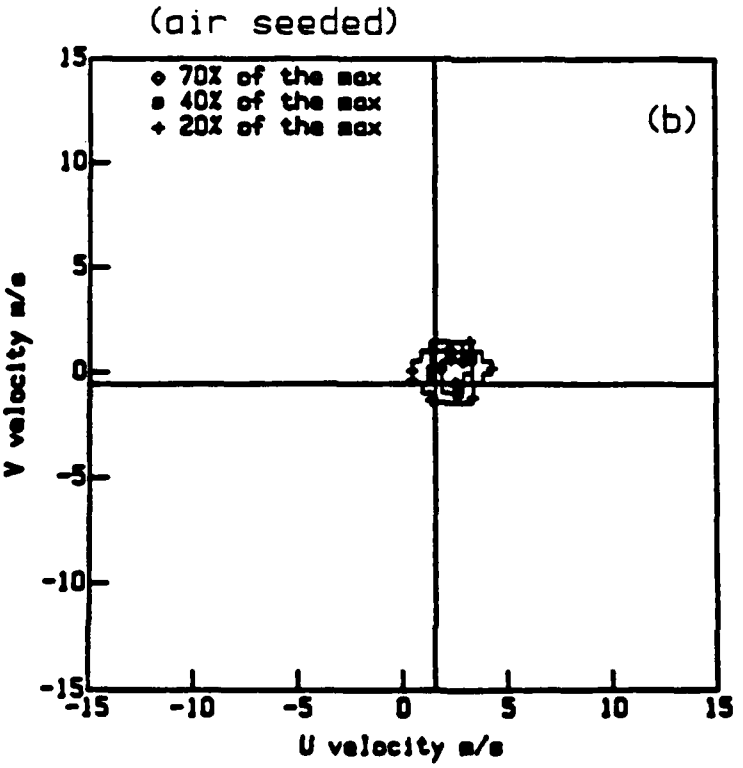

Fig 5

JPDF (U, V) AT X=-90mm ACROSS THE SHEAR ZONE

(air seeded) (feul seeded)

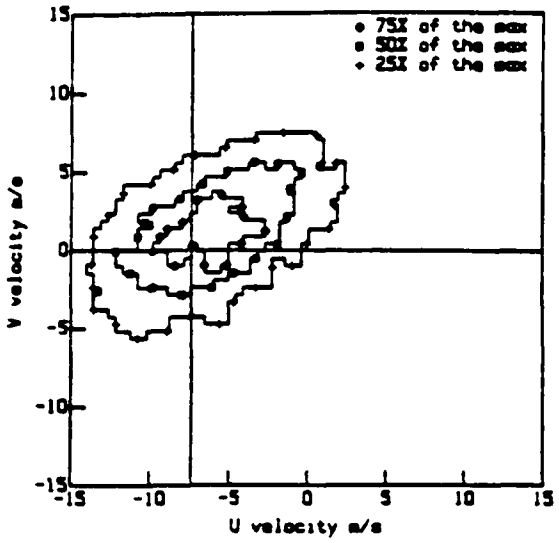

Y=-9mm

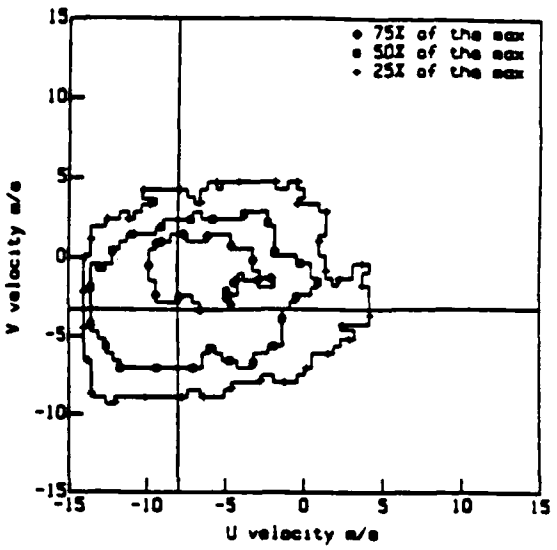

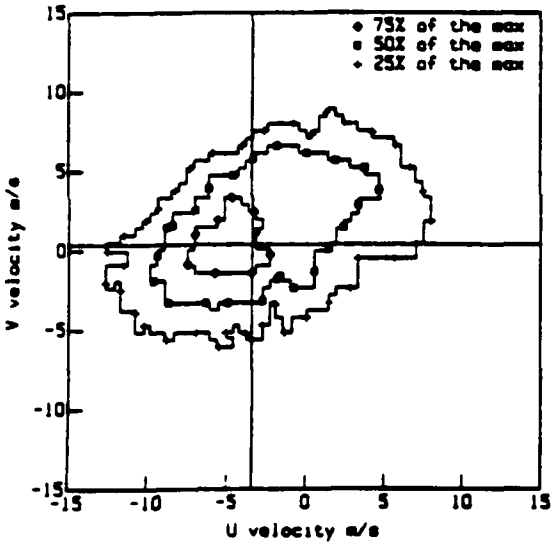

Y=-12mm

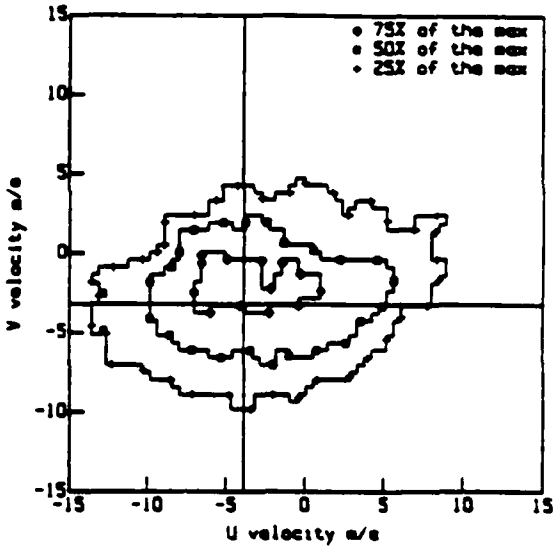

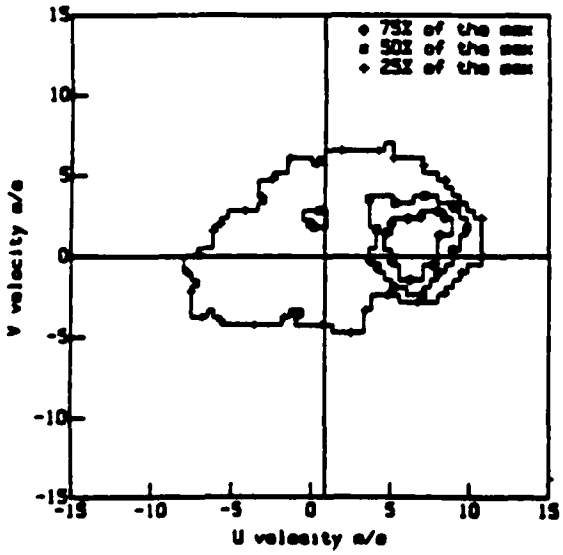

Y=-15mm

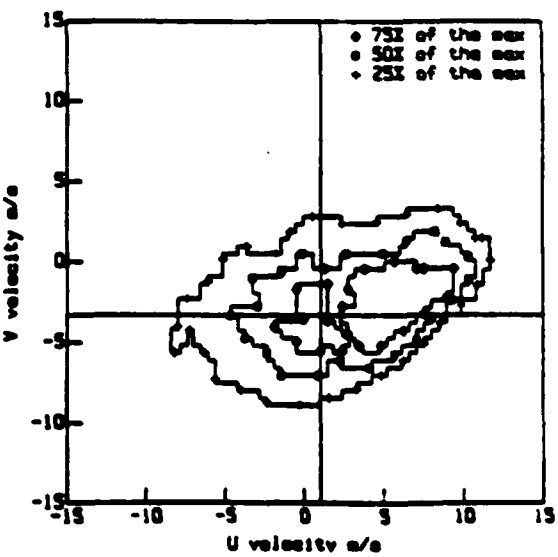

Fig 6

JPDF (U, V) AT X=-100mm ACROSS THE SHEAR ZONE

(air seeded)

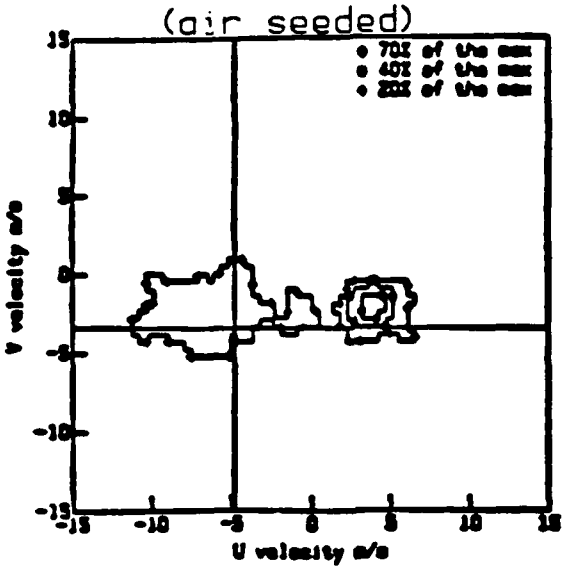

(fuel seeded)

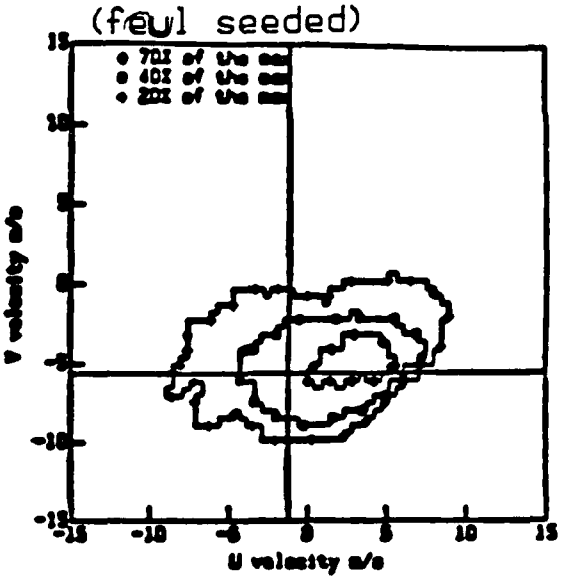

Y=-9mm

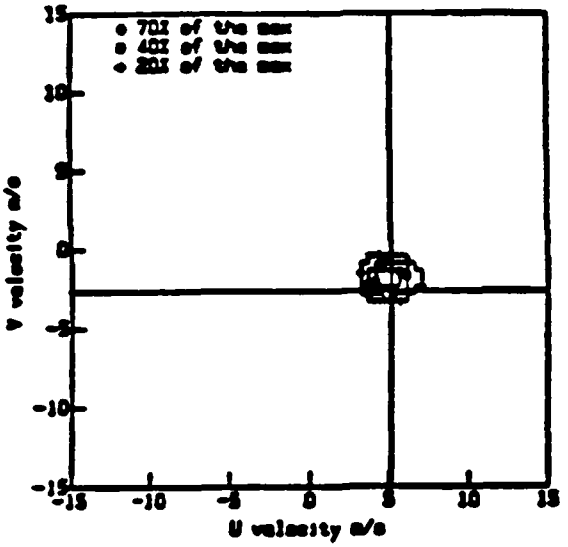

Y=-12mm

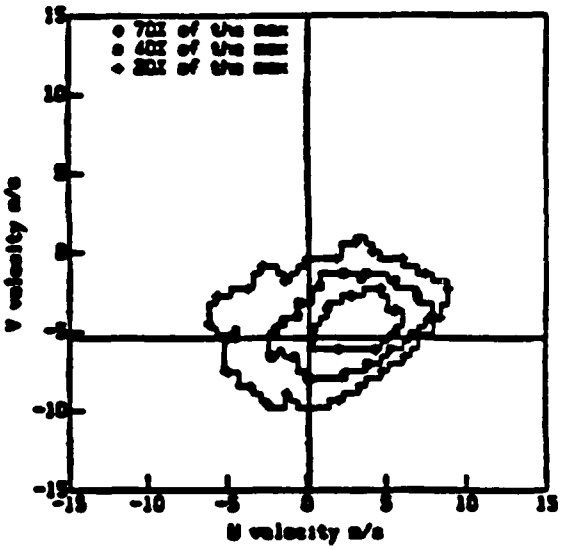

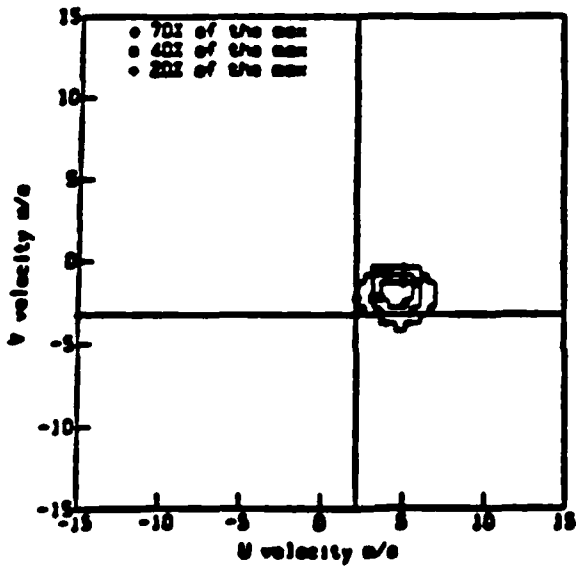

Y=-15mm

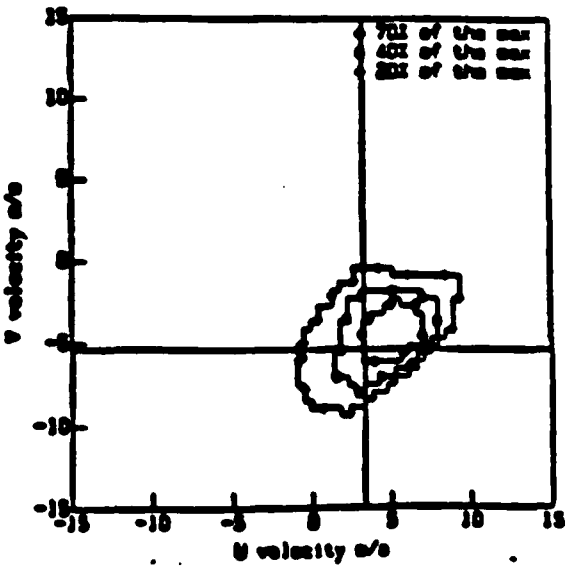

Fig 7

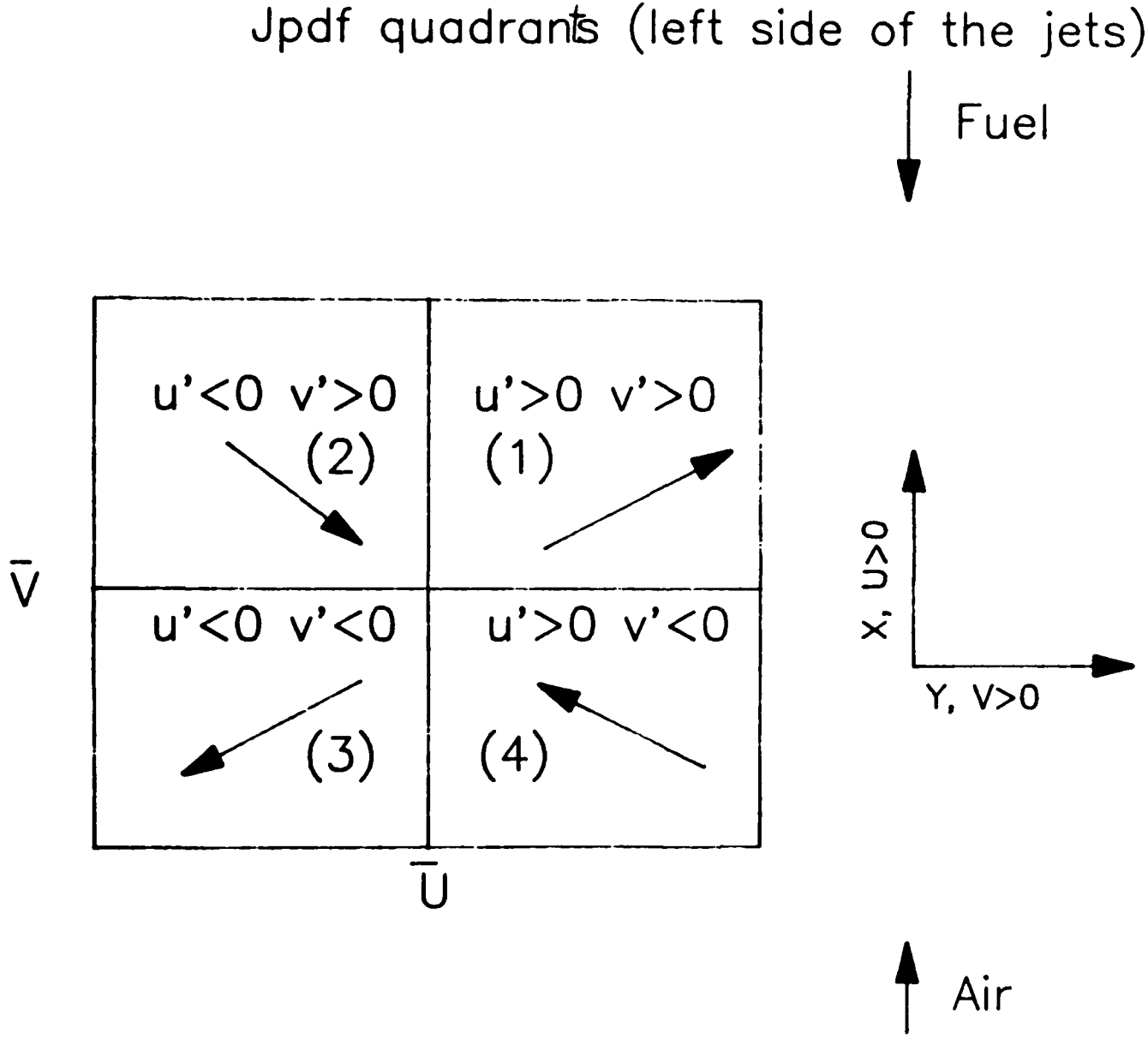
Jpdf quadrants (left side of the jets)
Fuel
u'<0 v'>0
(2)
u'>0 v'>0
(1)
u'<0 v'<0
(3)
u'>0 v'<0
(4)
V̄
Ū
X, U>0
Y, V>0
Air

Figure 8

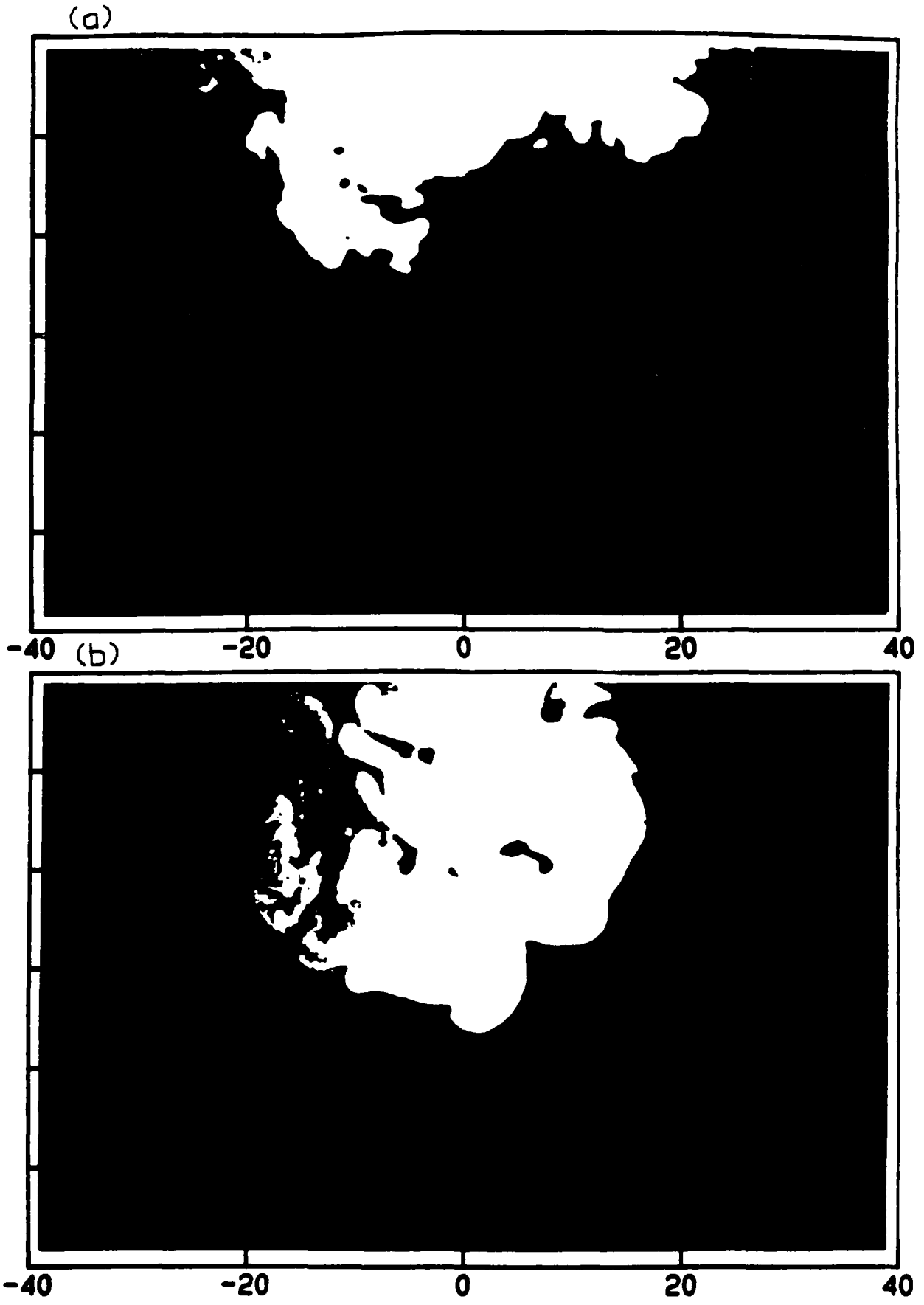

Fig 9

FRACTAL PLOTS OF THE FUEL SIDE OF THE REACTION ZONE

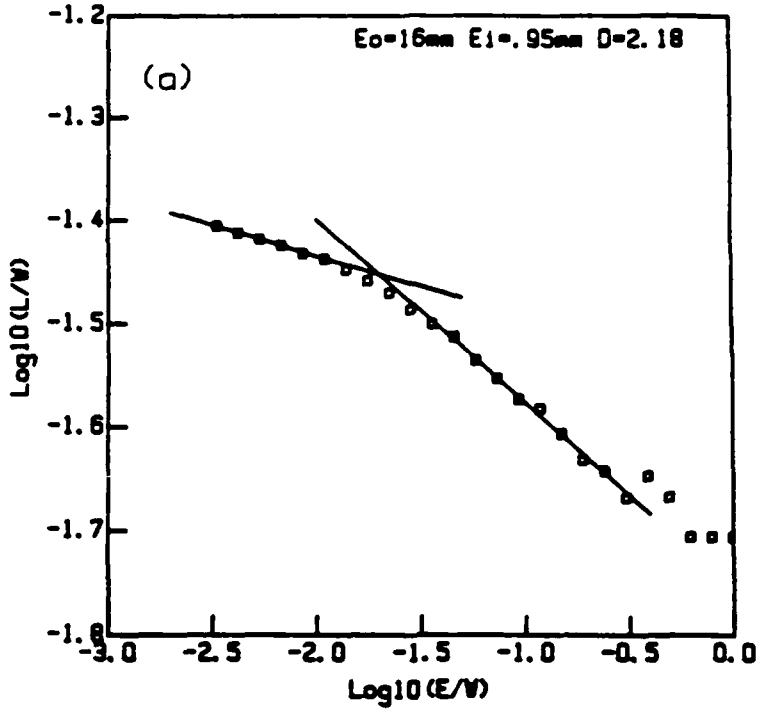

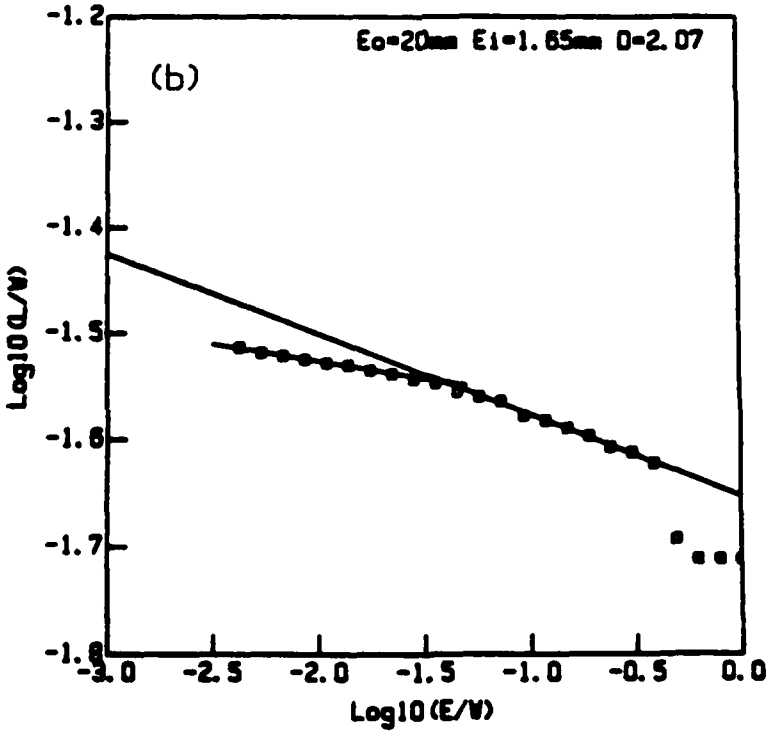

Fig 10

(a) t=0

(b) t=.57ms

Fig 11

PDF OF POSITION OF T=480 K (air side)

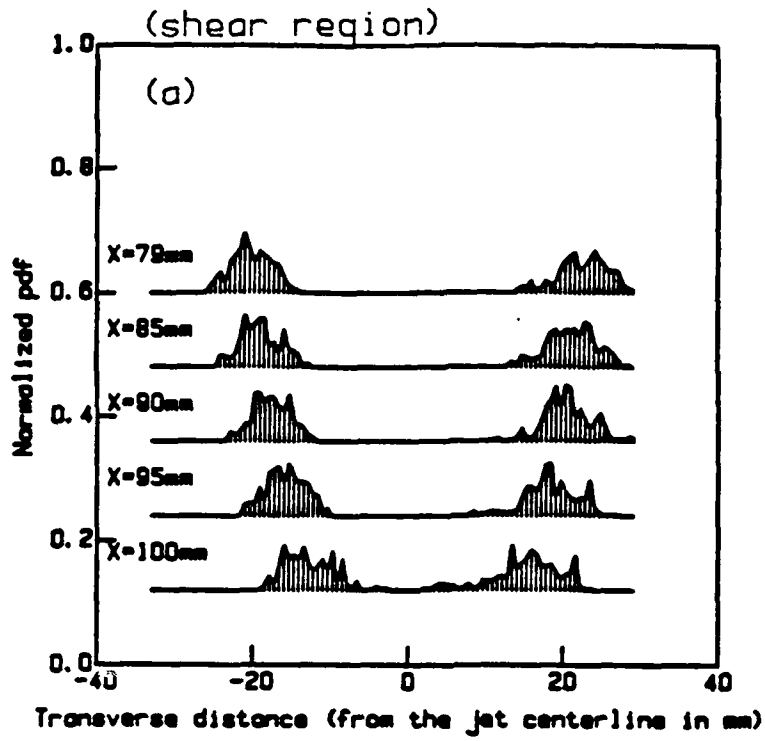

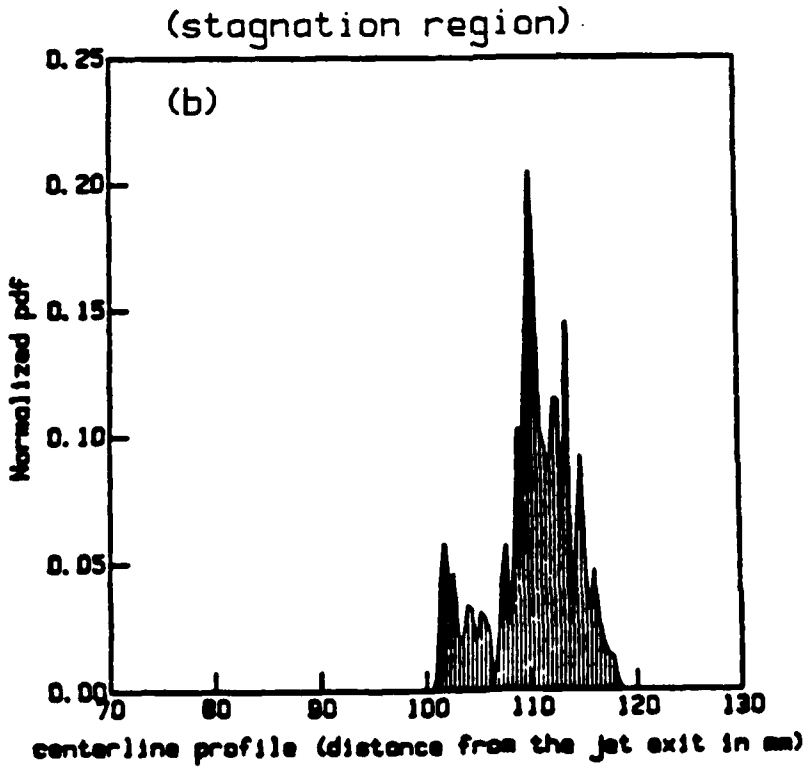

Fig 12

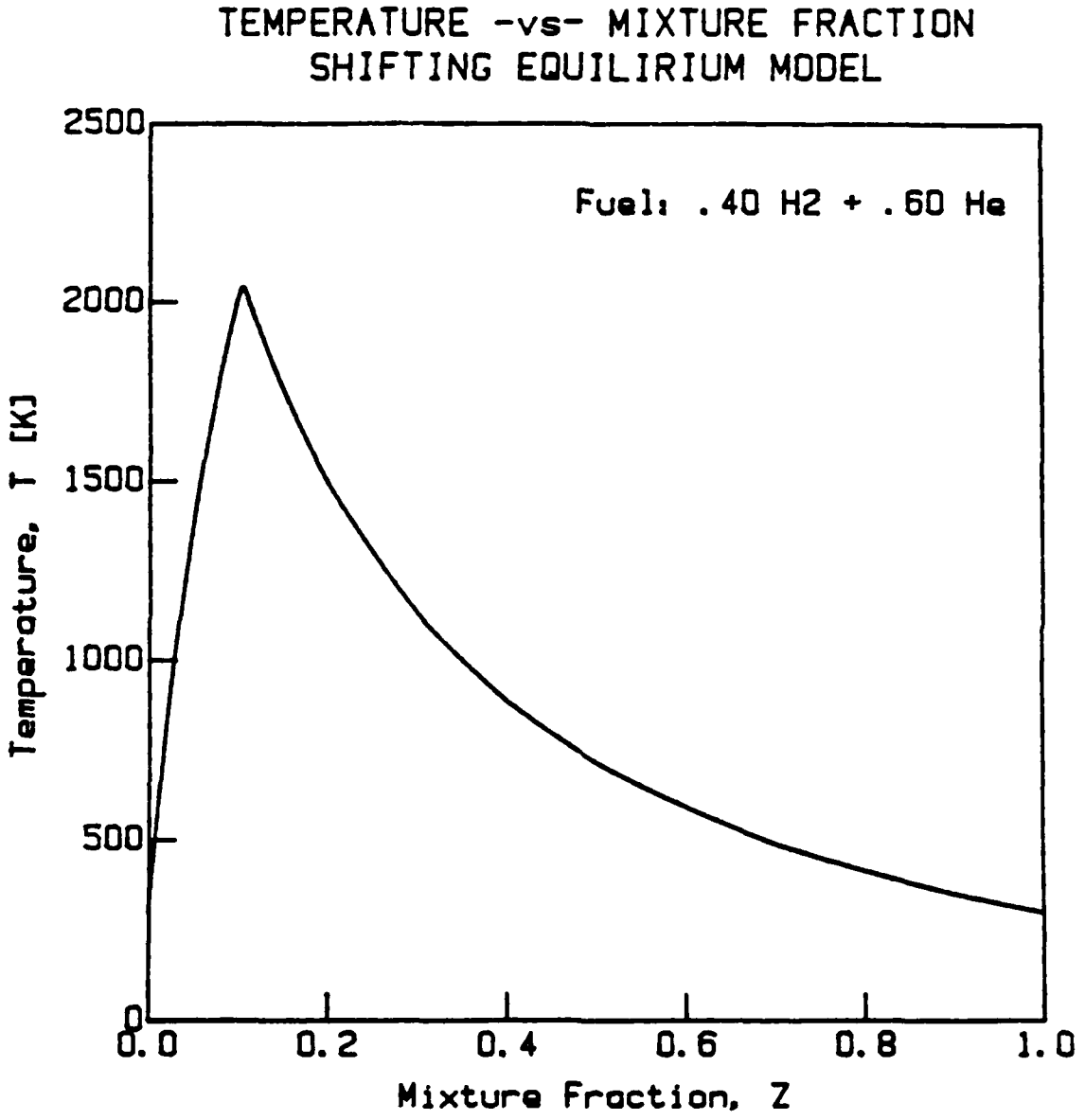
TEMPERATURE -vs- MIXTURE FRACTION
SHIFTING EQUILIRIUM MODEL
Fuel: .40 H2 + .60 He
Temperature, T [K]
2500
2000
1500
1000
500
0
0.0
0.2
0.4
0.6
0.8
1.0
Mixture Fraction, Z

Fig 13

ANALYTICAL REACTION ZONE THICKNESS DETERMINATION

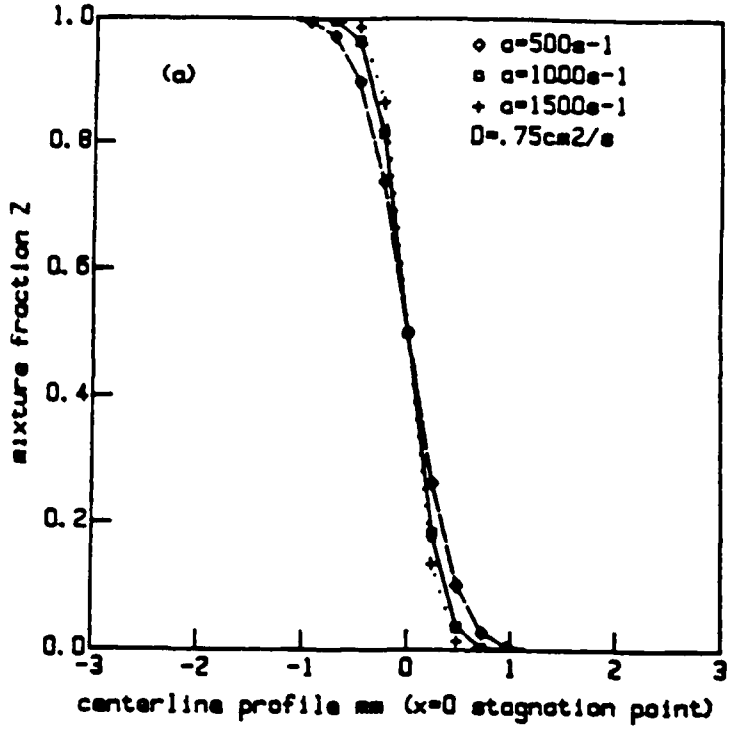

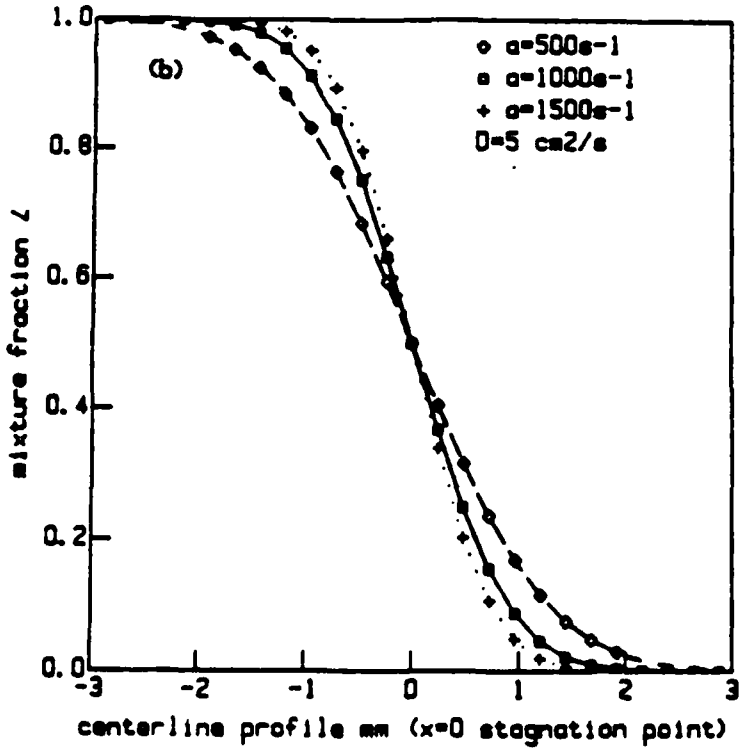

Fig 14

Direct Measurement of Mixture Fraction in Reacting Flow Using Rayleigh Scattering

P.J. Goix, K.R. Leonard, L. Talbot and J.Y. Chen (*)

Mechanical Engineering Department,
U.C. Berkeley, CA 94720.

(*) Sandia National Laboratory CRF,
Livermore, CA 94550.

Correspondent Authors : P. J. Goix

Lawrence Berkeley Laboratory B 29C

1 Cyclotron Road

Berkeley CA 94720

(415) 486 5438

Subjects:

(10) Flames

(5) Diagnostic Method

(27) Turbulent Reacting Flows

Abstract

The mixture fraction variable, ξ, is very useful in describing reaction zone structure in non-premixed flames. Extinction limits and turbulent mixing are often described as a function of this variable. Experimental evaluation of ξ is valuable in understanding the influence of turbulent mixing on the chemistry process. Historically, the evaluation of mixture fraction in combusting flow has required multiple concentration measurements. Here, a fuel has been designed to permit the measurement of the mixture fraction using only Rayleigh scattering. A Rayleigh intensity/ mixture fraction correspondence has been obtained experimentally in a laminar coflow flame. The influence of strain rate and differential diffusion effects has been investigated using a laminar counterflow diffusion flame and shifting equilibrium models. The results obtained from these comparisons are very encouraging and suggest that the Rayleigh/ mixture fraction correspondence established is valid under both turbulent mixing and laminar strained flamelet combustion regimes.

Introduction

The conserved scalar approach has been established to be most useful for describing the reaction zone structure of turbulent non-premixed flames. Bilger [1-2], under assumptions of unity Lewis number and constant mass diffusivity coefficients, has shown that turbulent mixing in the reaction zone can be modeled by the mixture fraction. Furthermore it has been demonstrated by several authors [2-4], that the reaction rate, which is the relevant quantity to study in turbulent-combustion interaction process, is a function of χ, the mixture fraction dissipation rate. Peters [3], has suggested that extinction limit conditions of turbulent non premixed flames can be expressed in terms of χ. In order to validate these theories considerable experimental mixture fraction data are still needed. Dibble et al. (6) have developed a method to measure the mixture fraction in a coflow turbulent diffusion flame. This point measurement method involves rather complicated and costly laser diagnostic techniques combining Rayleigh scattering and multichannel spontaneous Raman scattering. In this paper we describe a very simple method to measure mixture fraction using only Rayleigh scattering. This method is based on the choice of a fuel providing a monotonic relationship between the Rayleigh scattering signal and the mixture fraction variable. The influences on this

relationship of differential diffusion effects and strain effects, in particular close to the extinction limit, are also examined.

Fuel Design

Rayleigh scattering has been used extensively over the past fifteen years as a diagnostic in turbulent combustion. Under isobaric conditions the Rayleigh signal can be expressed as a function of the temperature, T, the species mole fractions, X_i, and their scattering cross sections, σ_i, where K is a constant involving all the optical and photodetection parameters.

$$I_R = \frac{K}{T}\sum_{i=1}^{i=n}\sigma_i X_i \tag{1}$$

Dibble et al [6], have shown that depending on the fuel design the Rayleigh signal across a combustion zone can provide different types of information. If, for example the average Rayleigh cross section $\sum_{i=1}^{i=n}\sigma_i X_i$ remains constant across the flame zone then the Rayleigh signal is inversely proportional to the temperature. This turns out to be the case for a mixture of 38% methane and 62% hydrogen burning in the air. On the other hand, if the average Rayleigh cross-section divided by the average molecular weight is constant across the flame then the Rayleigh signal is proportional to the density, which is the case for a mixture of 78% hydrogen an 22% argon burning in the air. Neither of these mixtures in combustion (due to temperature effects) lead to a mixture fraction measurement using Rayleigh technique.

Using a shifting equilibrium model (S.E.M) one can determine the temperature and mole fraction profiles in the mixture fraction space for a given fuel/oxidant mixture and then from known Rayleigh scattering cross sections [7], calculate the Rayleigh intensity as a function of $\vec{F}$ using Eq(1). Under combustion conditions for most fuels the Rayleigh signal is generally bimodal in mixture fraction around the stoichiometric value where the temperature is maximum. This is the case for the propane mixture used by E. Effelsberg and N. Peters (9). They used time series point measurements and the Taylor hypothesis to determine whether the Rayleigh signal corresponded to the lean or the rich side of the reaction zone. In this case the Rayleigh cross section of propane is 14 times the air Rayleigh cross section and the dynamic range one has to resolve between the product and the fuel in order to have a good signal/noise ratio over

the whole mixture fraction range, is about 100. Another problem concerning propane fuel is that under highly turbulent mixing conditions the flame becomes sooty and therefore the Rayleigh signal is severely contaminated. The fuel mixture that we propose here (85% helium,15% hydrogen) has a smaller mean Rayleigh cross section than the combustion products. Then as shown in Fig. 1 the Rayleigh intensity signal across the flame in mixture fraction space is a monotonic function and the mixture fraction can be determined without ambiguity from a Rayleigh measurement. The Rayleigh signal ratio between the pure air side $\xi = 0$ and the pure fuel side $\xi = 1$ is found to be 22. One can note significant differences in the curve sensitivity for the range of mixture fraction $\xi = 0$ to $\xi_s = .25$ (air side) and $\xi_s = .25$ to $\xi = 1$.. The problem arising here is to be able to measure accurately the Rayleigh intensity with a good signal/noise ratio within the full mixture fraction range.

Experimental set up and Rayleigh measurements

In order to investigate the Rayleigh scattering properties of the chosen helium-hydrogen mixture, a laminar coflow diffusion flame was set up. The burner consisted of a fuel pipe of 6 mm in diameter surrounded by a coflowing air flow of 30mm diameter. The fuel jet Reynolds number was Re=500. The helium volumetric concentration (85%) in the fuel jet was controlled by a calibrated flow meter. The Rayleigh measurement set up is shown Fig (2). A focused laser beam from a copper vapor laser is directed across the flame using a classical two lens system. The beam waist diameter is .3mm over a length of 10 mm. The cooper vapor laser is capable of a repetition rate of 10khz with pulse duration of 20ns and 5mJ energy. The Rayleigh light scattered at 90 degree is spatially filtered and imaged on the pinhole of a photomultiplier using a 50mm f 1/1.8 lens. The amplified output of the photomultiplier is fed through a box car integrator. The box-car is triggered with appropriate time delay and set to integrate over only the 20 ns duration of the laser pulses, thus eliminating noise problems such as flame and background radiation between pulses. The photomultiplier linearity was checked for the range of the operating conditions. For each measurement the laser pulse energy value is recorded and ratioed to the Rayleigh scattering signal value. Fig. 3 shows a Rayleigh signal radial intensity profile obtained at 10mm from the coflow burner exit. Two profiles 1mm above and below the laser beam were also recorded, in order to evaluate the aver-

age background intensity level. The profile of Fig. 3 shows clearly the monotonic behavior of the normalized signal $I^*_R = \frac{(I_R - I_{Rmin})}{(I_{Rmax} - I_{Rmin})}$ from the air side to the fuel side. One can also note the small background contribution on the signal level. Fig. 4 shows the evolution of the variance of the Rayleigh intensity signal versus its average. The Rayleigh signal probability distribution at each point was found to be gaussian and the linear relationship between I_R and its variance indicates that the photon count rate obeys Poisson statistics. This result is important for future measurement in turbulent conditions, where the noise can be modeled as a function of the average Rayleigh signal intensity value.

Rayleigh measurements in Mixture Fraction Space

Laminar, one dimensional diffusion flame structure has been studied quite extensively recently (11,14). In particular, the influence of the flow field strain on the reaction zone structure is quite well known in the case of hydrogen chemistry (12). The models employed in these studies provide both spatial and mixture fraction concentration profiles under different strain rate conditions. A common configuration used to compute the one dimensional flame is the Tsuji burner. One very important parameter in this configuration is the velocity gradient across the reaction zone which is the convection term of the problem. When this convection term and hence the strain rate is increased, a limit exists beyond which the flame cannot be sustained and it extinguishes. When the strain rate is very low the problem is a one dimensional molecular diffusion driven problem. In this case (low strain rate), it is reasonable to assume that the flame structure in mixture fraction space is the same as that of a coflow laminar diffusion flame, which is also a molecular diffusion driven flame. Fig. 5 represents the laminar flame structure in mixture fraction space for the Tsuji burner configuration under low strain rate condition $a = 10s^{-1}$ for the chosen 85%He/15%H2 fuel. On this figure are plotted the mass fractions of the species having significant contribution to I_R. From those mass fraction profiles and the Rayleigh cross section values found in the literature (5), one can compute the I_R^* profile of the flame as shown in Fig. 6. One can note that both the modeled I^*_R profiles (Fig. 6 Tsuji burner) and the one measured from the coflow burner Fig. 3 exhibit the same features. They are both monotonically decreasing with ξ and present a maximum Rayleigh intensity gradient on the air side. The main difference in the two profiles is the thickness of the reaction zone. In the stagnation case the

convection and the diffusion fluxes are parallel to each other while for the coflow burner these fluxes are perpendicular which causes the reaction zone in the coflow case to be thicker and also a function of downstream distance from the burner exit. Hence, to compare the measured and computed I^*_R profiles in terms of the space/mixture fraction correspondence we have rescaled the profiles of Fig. 6 and Fig. 3 using the maximum I^*_R gradient thickness as characteristic of the two profiles. Fig. 7 represents the comparison of the two profiles thus rescaled using the maximum gradient thickness for normalization. One can note very good agreement between the model and the data. Then, using the space/mixture fraction correspondence provided by the model one can now compare the Rayleigh intensities measured and predicted in mixture fraction space. Fig. 8 shows the excellent agreement between prediction and experiment under the low strain condition $a = 10s^{-1}$. It is also worth noting that the region of ξ where the curves were forced to match (maximum I^*_R gradient) corresponds only to a range in mixture fraction less than .1 located on the air side of the reaction zone where differential diffusion effects are expected to be of secondary importance, as discussed below.

Strain rate and differential diffusion effects

Figure 8 shows clearly the very good agreement between the predicted and measured I^*_R in mixture fraction space. The question that we next address is to what extent strain rate may affect this agreement. Fig. 9 shows the reaction zone structure of the Tsuji type flame for our hydrogen/helium fuel mixture computed very close to the extinction limit at a strain rate of $a = 190s^{-1}$. The maximum temperature is decreased by about 300K in comparison with the low strain rate case. From these profiles ($a = 190s^{-1}$), one can compute the corresponding I^*_R signal and compare it to the low strain rate condition as shown Fig. 10. Once again even if the reaction zone concentration profiles are quite sensitive to the strain rate value, I^*_R in the mixture fraction space remains the same. This result is very encouraging and indicates that the Rayleigh/mixture fraction correspondence determined earlier is practically independent of the strain rate, and thus it should be possible to measure the mixture fraction across the reaction zone of a laminar strained flamelet. Bilger has shown that mixture fraction variable is very well suited to the study of the turbulent mixing occurring in the reaction zone. When the mixing is highly turbulent, molecular

effects are found to be negligible and the hypotheses of unity Lewis number and constant diffusivity coefficients are more acceptable. Laboratory experiments are very often made at moderate Reynolds number and molecular transport effects can have significant contributions. For our fuel the mass diffusivities of nitrogen, oxygen and hydrogen, helium are very different and differential diffusion effects are expected to be significant [15]. Figure 11 shows for comparison the I^*_R variation with mixture fraction using the Shifting Equilibrium Model (S.E.M) and the laminar one dimensional model (where differential diffusion effects are included). Here again the differences between the two models are quite small. Mixture fraction measurements using Rayleigh scattering for our chosen Hydrogen/Helium mixture are very promising, particularly for turbulent flows where the effects associated with differential diffusion will be of lesser importance compared with turbulent transport which can only be approximated in currently available turbulence models. The guidance provided by measurements made with our particular fuel could be used to improve turbulence modeling of combustion involving more practical fuels.

Summary

A fuel consisting of 85% helium and 15% hydrogen has been designed to make possible the experimental determination of the mixture fraction. For this specific fuel the Rayleigh intensity signal is a monotonic function of the mixture fraction. Rayleigh measurements have been carried out on a laminar coflow burner using this fuel. The results show that the Rayleigh intensity can be measured with a very good signal noise ratio for the entire mixture fraction range. A laminar counterflow flame model has been used to transform the spatial measurements in mixture fraction space and also to study the influence of strain rate on the Rayleigh/mixture fraction correspondence, (particularly, close to extinction), which has been found to be negligible. A comparison of the laminar counterflow model with the shifting equilibrium model indicates that differential diffusion effects have little influence on the Rayleigh/mixture fraction relationship. These results indicate that mixture fraction measurements can lead to accurate results, both for highly turbulent diffusion flames and laminar strained flamelets, of significant value to the modeling of these flames.

Acknowledgement

The authors would like to acknowledge Prof. R. W. Bilger of the University of Sydney who gave birth to this idea during his tenure as a visiting Professor at U.C. Berkeley. The authors would like also to express their appreciation to Dr. R.K. Cheng, Dr. I.G Shepherd and Mr. G.L. Hubbard for their assistance in the experimental set up and useful discussions. This research was supported by the Air Force Office of Scientific Research under the Contract AFOSR-88-0011, and one of the authors (JYC) was supported by U. S. the Department of Energy, Basic Energy Sciences, Division of Chemical Sciences. The experiments were conducted at the Lawrence Berkeley Laboratory with equipment supported by the Director, Office of Energy Research, Office of Basic Energy Sciences, Chemical Science Division of the U. S. Department of Energy under contract No. DE-AC-03-76SF00098.

References

(1) Bilger, R., 22nd Symposium Int'l on Combustion 1988 Seattle, pp 475-488.

(2) Bilger, R., *Combustion Sciences and Technology* vol 13, no.1-6, 1976.

(3) Peters, N., *Progress in Energy and Combustion Science* vol 10 no 3 1983.

(4) Williams, F.A., "Combustion Theory" 2nd Edition. The Benjamin-Cummings Publishing Company, Inc. 1985.

(5) Namer, I., Schefer, R. W.,Chan, R.W., "Interpretation of Rayleigh Scattering in a Flame" Spring meeting of the Western States section/Combustion Institute, Irvine CA, April 21-22, 1980.

(6) Dibble, R.W, Hollenbach, R. E., 18th Symposium Int'l on Combustion. The Combustion Institute, pp 1489-1499 1980.

(7) Schefer, R.W., Dibble, R.W., AIAA 24th Aerospace Sciences Meeting, Reno, NV Jan 6-9, 1986.

(8) Kennedy, I. M.,Kent, J.H., 18th Symposium Int'l on Combustion pp, 279-288, 1980.

(9) Effelsberg, E., Peters, N., 22nd Symposium Int'l on Combustion Institute 1988, Seattle, pp 693-700

(10) Magre, P., Dibble, R.W., *Combustion and Flame*, vol 73 No 2 Aug 1988.

(11) Tsuji, H., *Progress Energy and Combustion Sciences*, vol. 8, pp93-119, 1982.

(12) Dixon-Lewis, G.,Missaghi, M. 22snd Symposium Int on Combustion/The Combustion Institute 1988.pp 1461-1470.

(13) Drake, M. C., Blint, R.J., *Combustion Sciences and Technology*, vol. 61, pp 187-224 (1988)

(14) Kee, R.J., Miller, J.A., Evans, G.H., Dixon-Lewis, G. 22nd Int'l Symposium on Combustion .pp 1479-1494, 1988 Seattle.

(15) Bilger, R. W., A.I.A.A., July 1982, pp 962-970.

Captions

Fig 1 Normalized Rayleigh signal prediction versus mixture fraction for a fuel of 85%helium ,15%hydrogen burning in the air, calculated using a shifting equilibrium model.

Fig 2 Rayleigh scattering experimental set up for a laminar coflow diffusion flame.

Fig 3 Normalized Rayleigh intensity profile obtained at 10mm from the burner exit.

Fig 4 Variance of the Rayleigh signal versus the average Rayleigh intensity signal obtained at 10mm of the laminar burner exit.

Fig 5 Reaction zone structure of the Tsuji flame for a strain rate $a = 10s^{-1}$.

Fig 6 Normalized Rayleigh intensity profiles deduced from Eq.(1) using the reaction zone prediction of Fig. 5.

Fig 7 Normalized Rayleigh intensity profiles comparisons rescaled using the maximum gradient thickness.

Fig 8 Comparison between predicted and measured normalized Rayleigh intensity profiles in mixture fraction space.

Fig 9 Reaction zone of the Tsuji flame for a strain rate $a = 190s^{-1}$

Fig 10 Influence of strain rate on the normalized Rayleigh intensity profile. (1) $a = 10s^{-1}$ (2) $a = 190s^{-1}$.

Fig 11 Comparison of the normalized Rayleigh intensity profiles in mixture fraction space for both laminar counterflow and shifting equilibrium models.

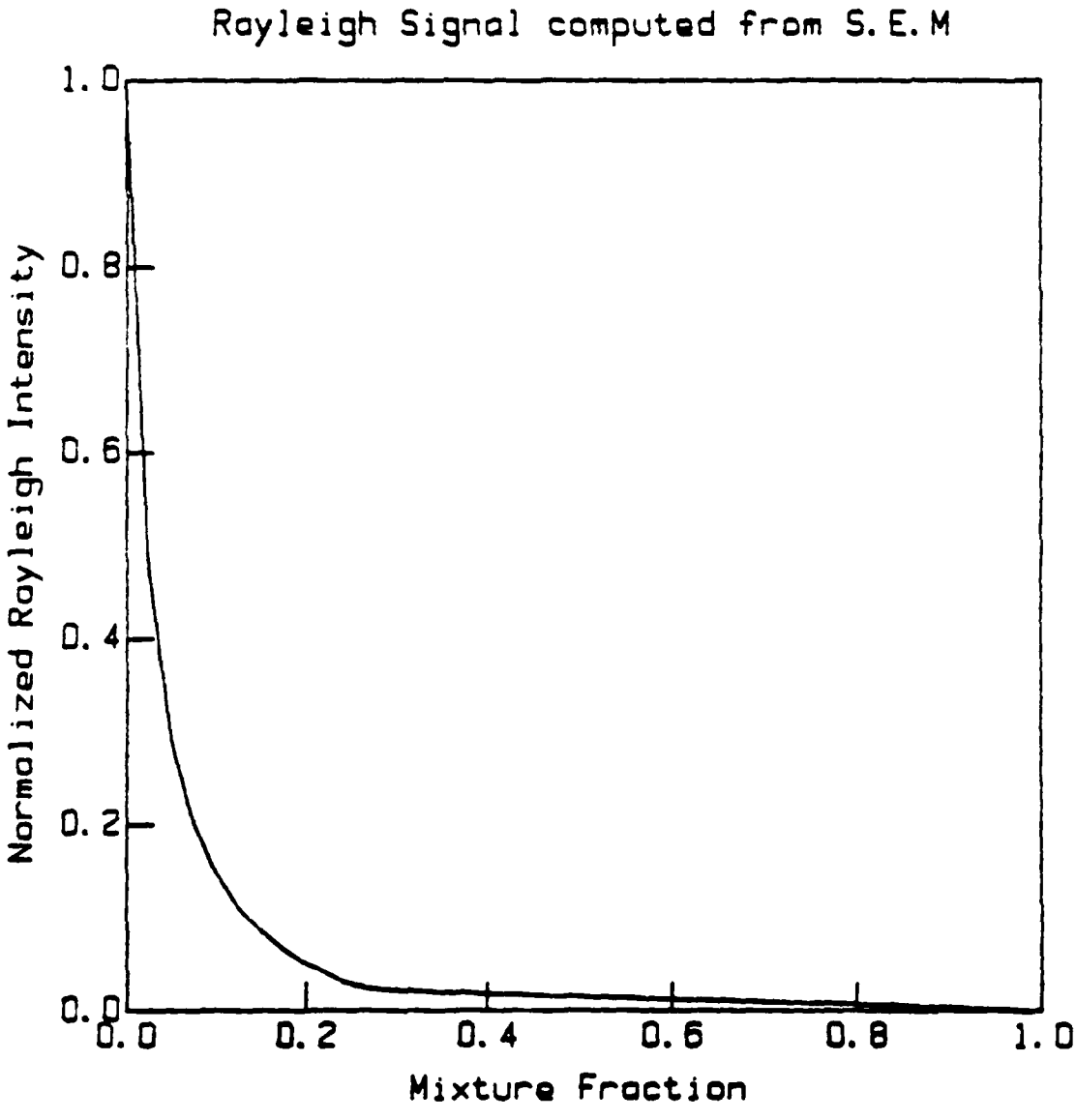
Rayleigh Signal computed from S.E.M
Normalized Rayleigh Intensity
1.0
0.8
0.6
0.4
0.2
0.0
0.0
0.2
0.4
0.6
0.8
1.0
Mixture Fraction

Figure 1

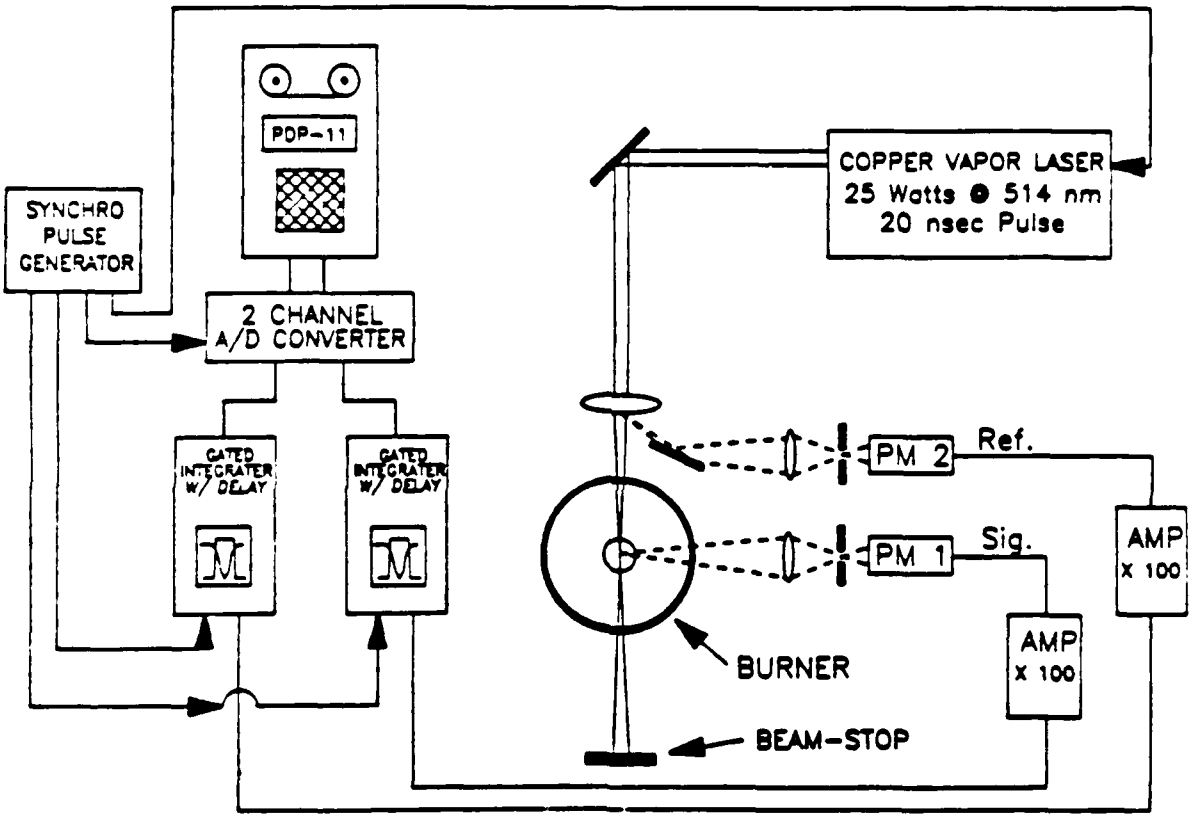

APPARATUS FOR MIXTURE FRACTION MEASUREMENTS

Figure 2

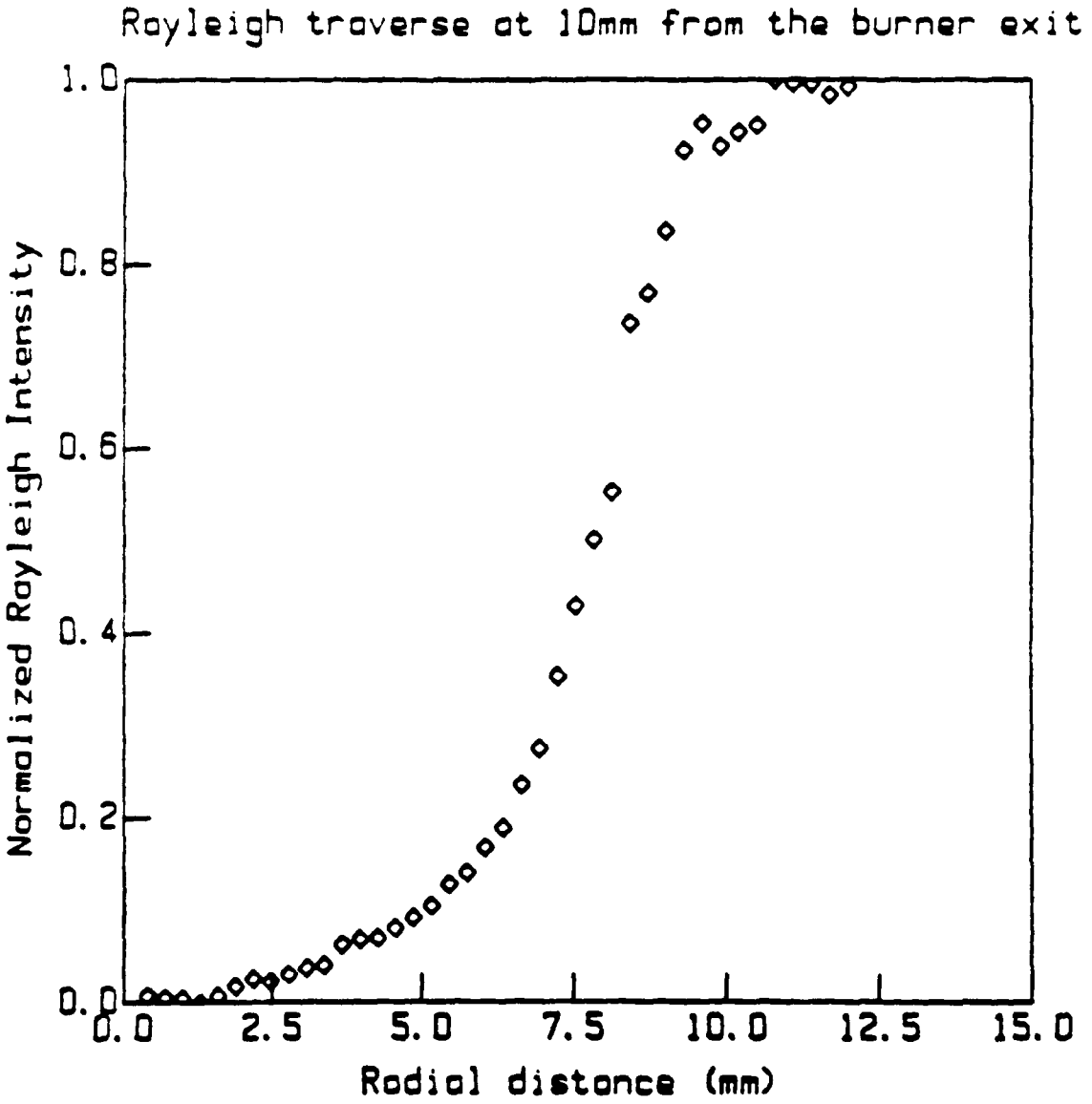
Rayleigh traverse at 10mm from the burner exit
Normalized Rayleigh Intensity
1.0
0.8
0.6
0.4
0.2
0.0
0.0
2.5
5.0
7.5
10.0
12.5
15.0
Radial distance (mm)

Figure 3

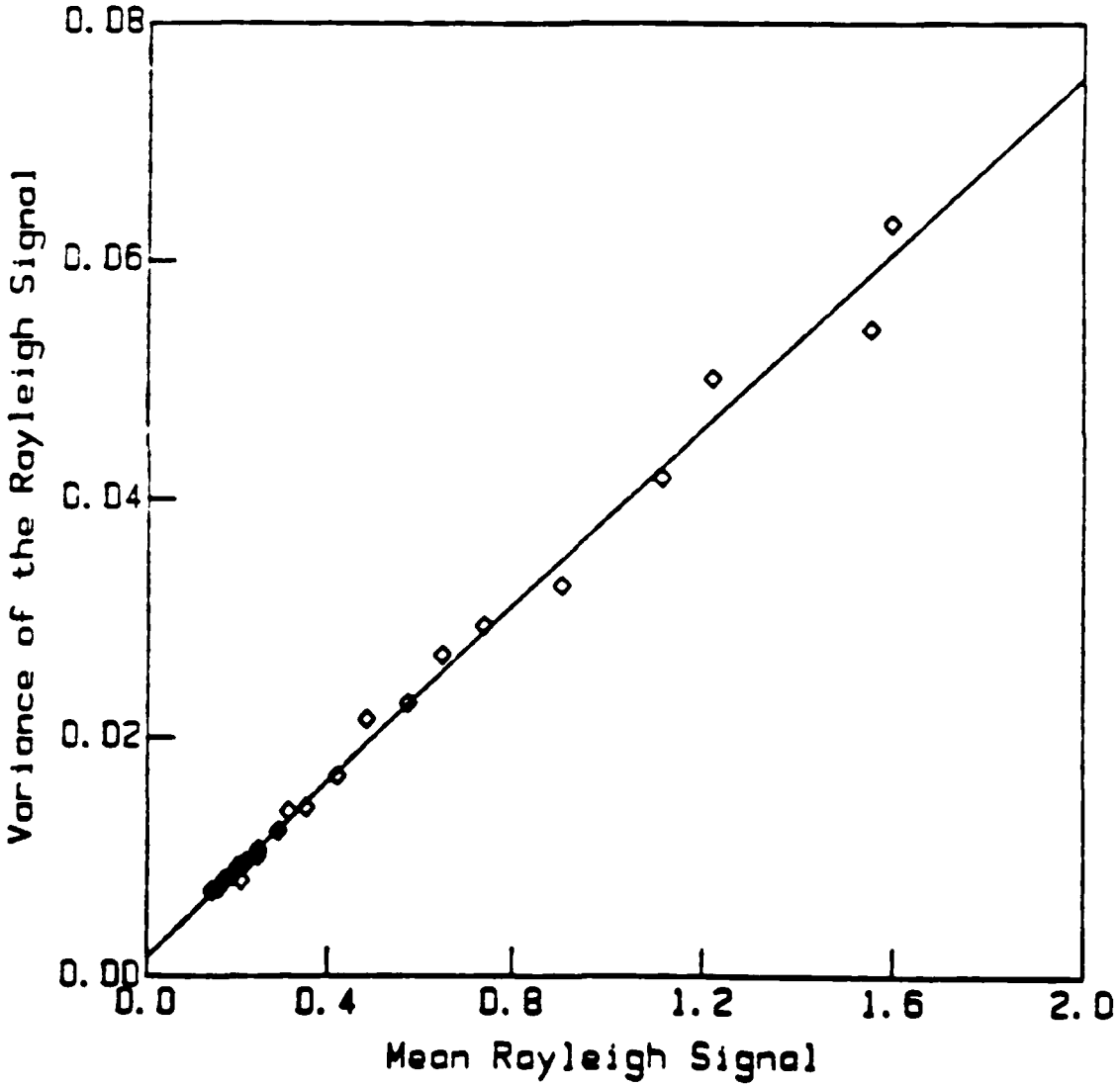
0.08
0.06
0.04
0.02
0.00
Variance of the Rayleigh Signal
0.0
0.4
0.8
1.2
1.6
2.0
Mean Rayleigh Signal

Figure 4

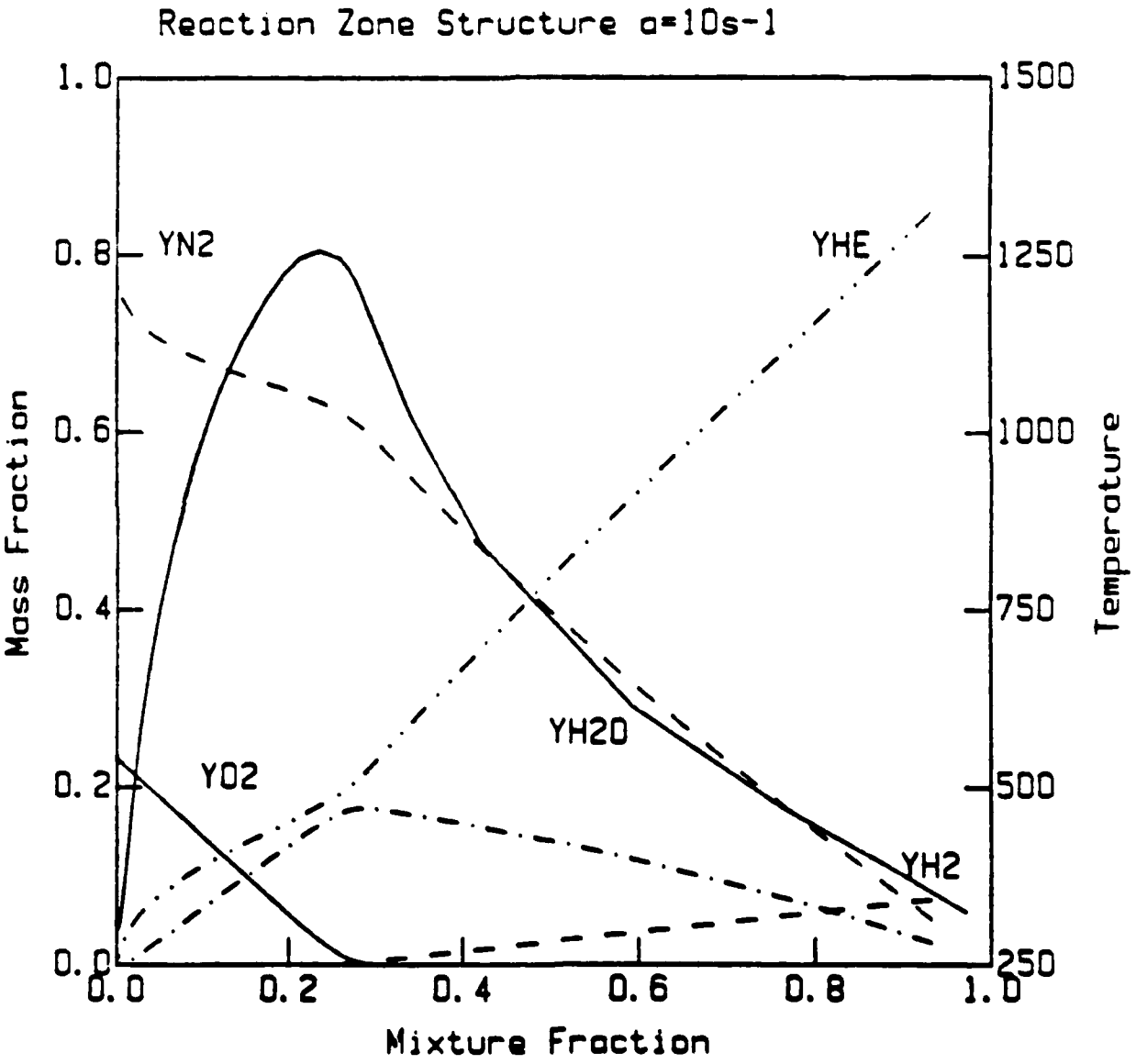
Reaction Zone Structure a=10s-1
1.0
0.8
0.6
0.4
0.2
0.0
Mass Fraction
1500
1250
1000
750
500
250
Temperature
YN2
YHE
YH2O
YO2
YH2
0.0
0.2
0.4
0.6
0.8
1.0
Mixture Fraction

Figure 5

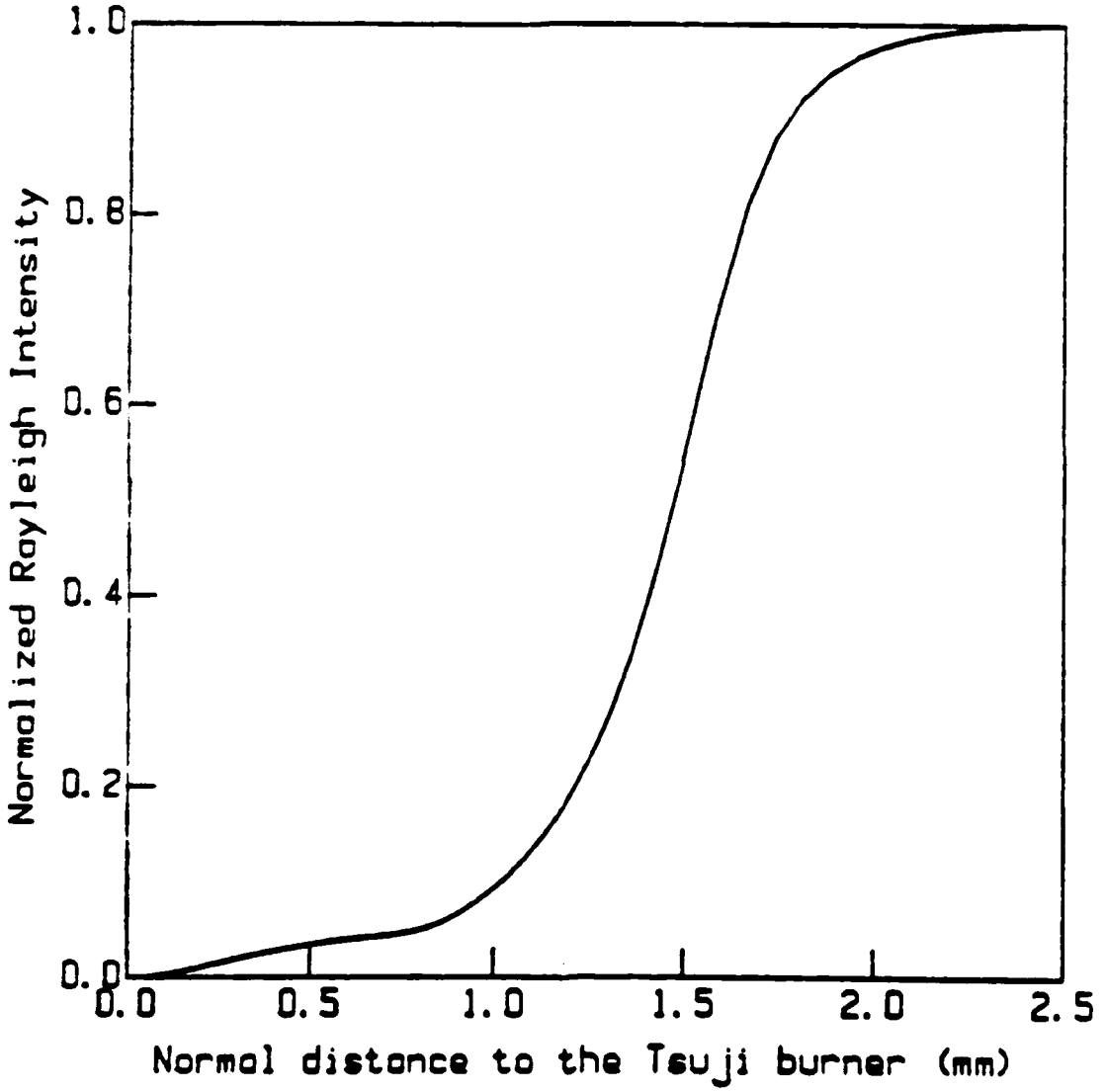
1.0
0.8
0.6
0.4
0.2
0.0
Normalized Rayleigh Intensity
0.0
0.5
1.0
1.5
2.0
2.5
Normal distance to the Tsuji burner (mm)

Figure 6

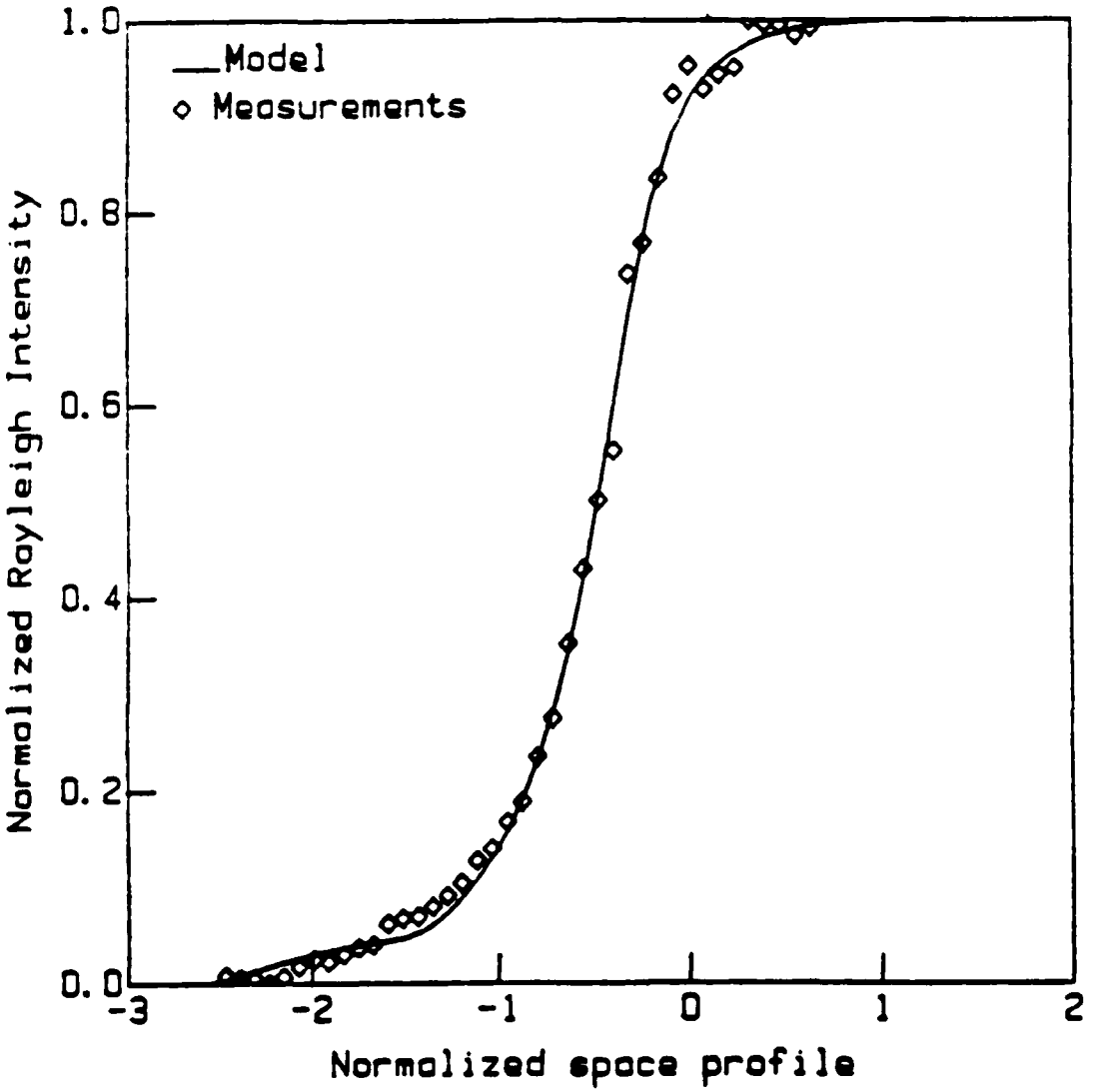
Model
Measurements
Normalized Rayleigh Intensity
1.0
0.8
0.6
0.4
0.2
0.0
-3
-2
-1
0
1
2
Normalized space profile

Figure 7

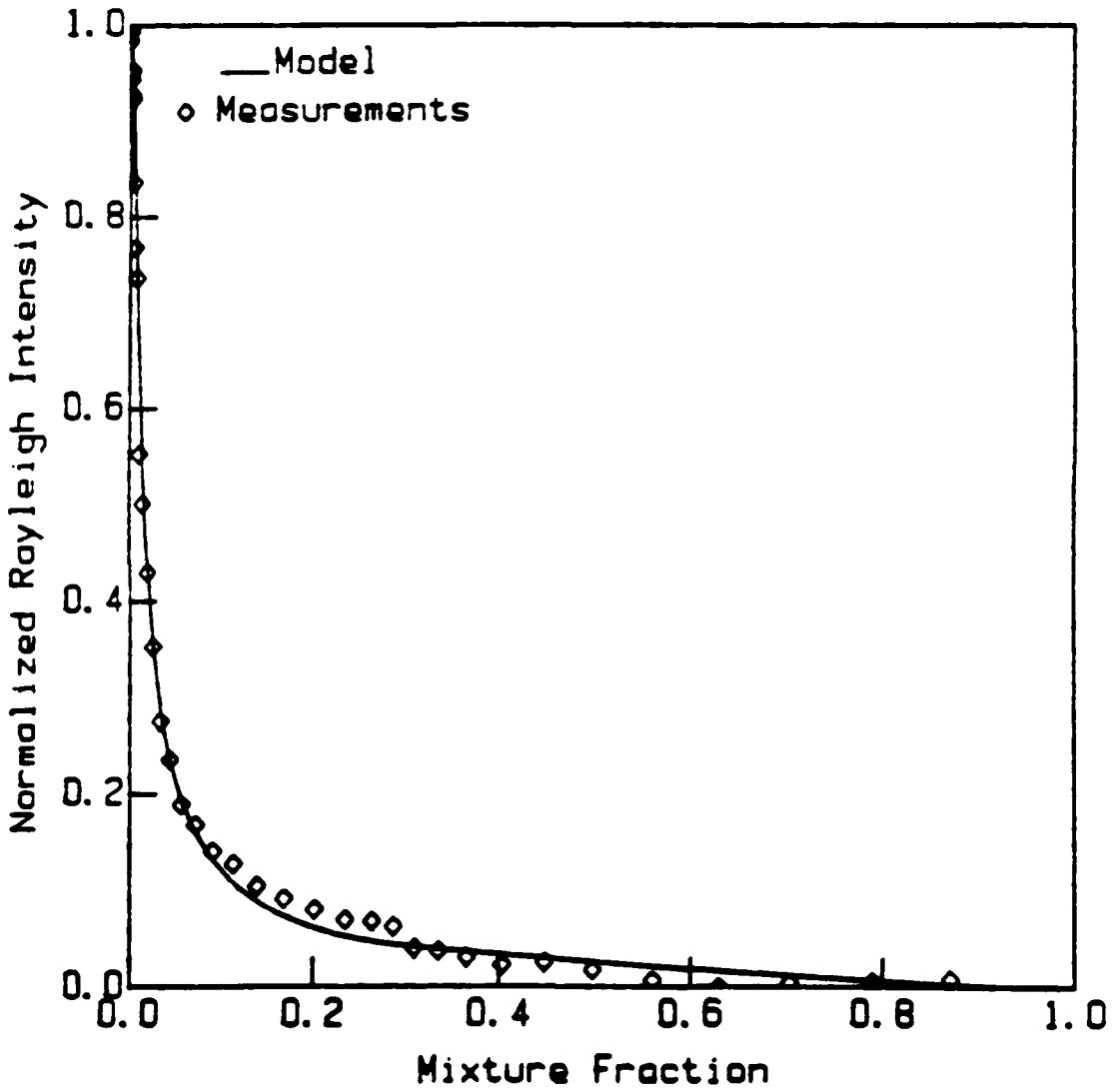
Model
Measurements
Normalized Rayleigh Intensity
Mixture Fraction
1.0
0.8
0.6
0.4
0.2
0.0
0.0
0.2
0.4
0.6
0.8
1.0

Figure 8

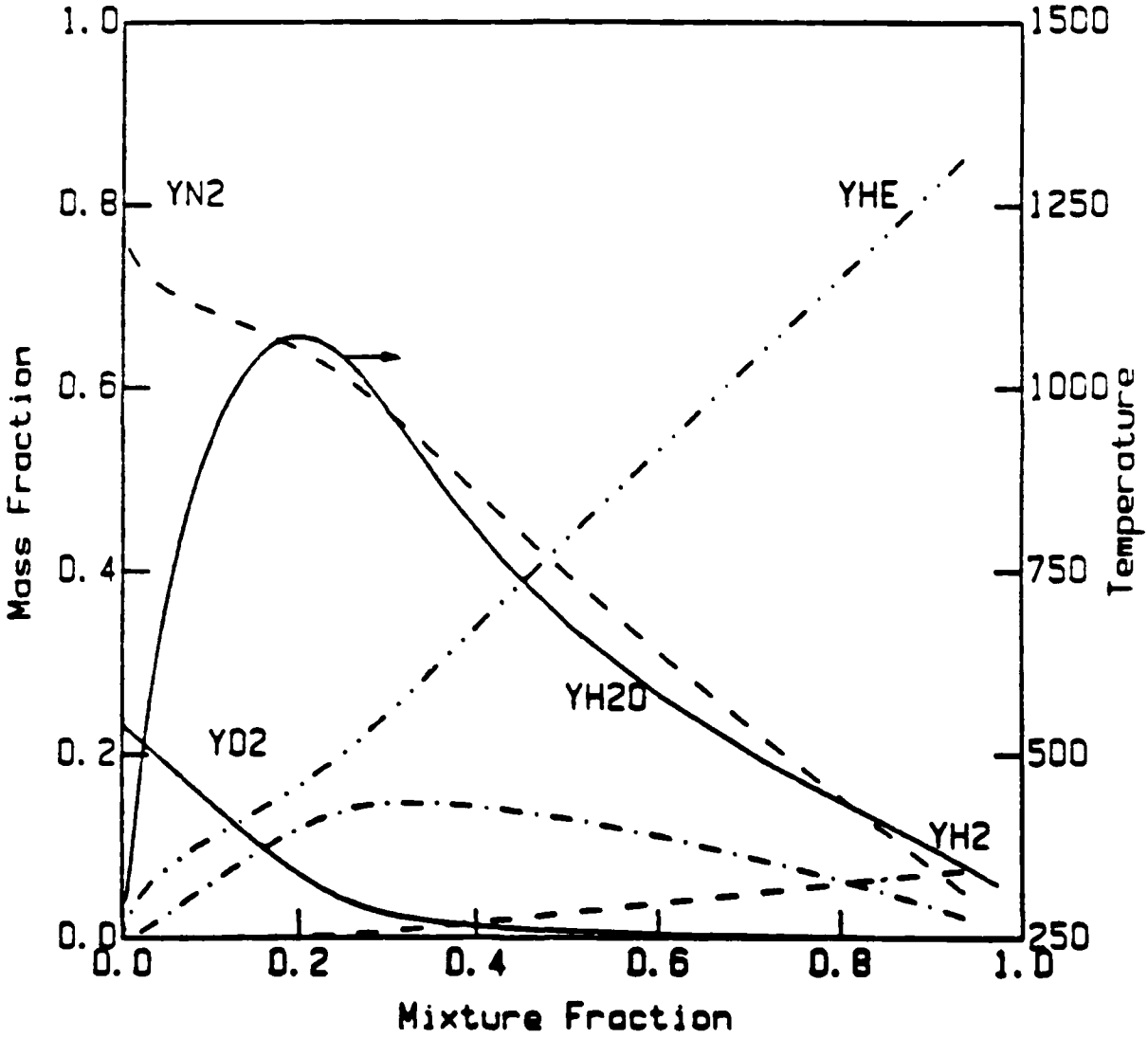
1.0
0.8
0.6
0.4
0.2
0.0
Mass Fraction
YN2
YHE
YH2O
YO2
YH2
1500
1250
1000
750
500
250
Temperature
0.0
0.2
0.4
0.6
0.8
1.0
Mixture Fraction

Figure 9

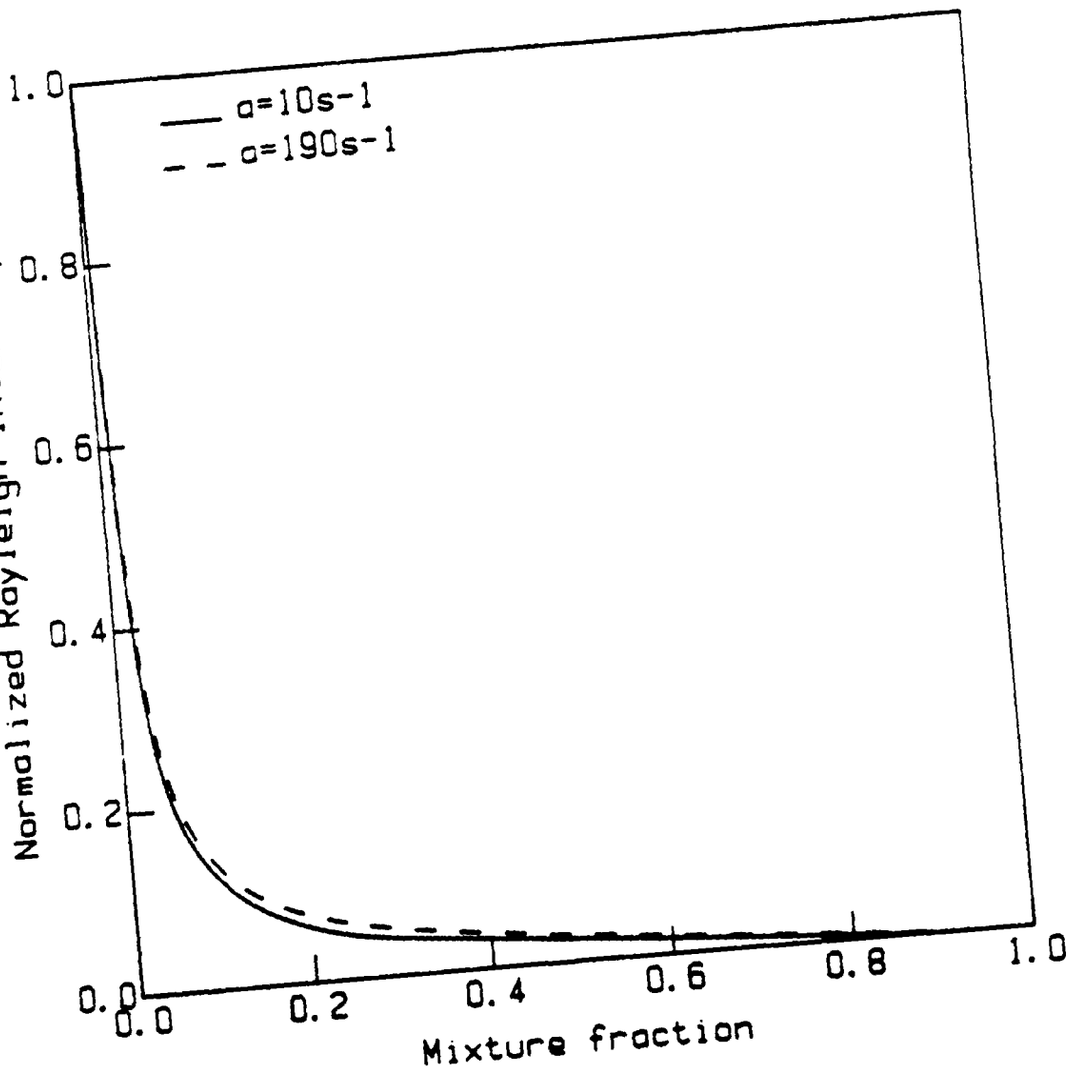
a=10s-1
a=190s-1
Normalized Rayleigh Intensity
1.0
0.8
0.6
0.4
0.2
0.0
0.0
0.2
0.4
0.6
0.8
1.0
Mixture fraction

Figure 10

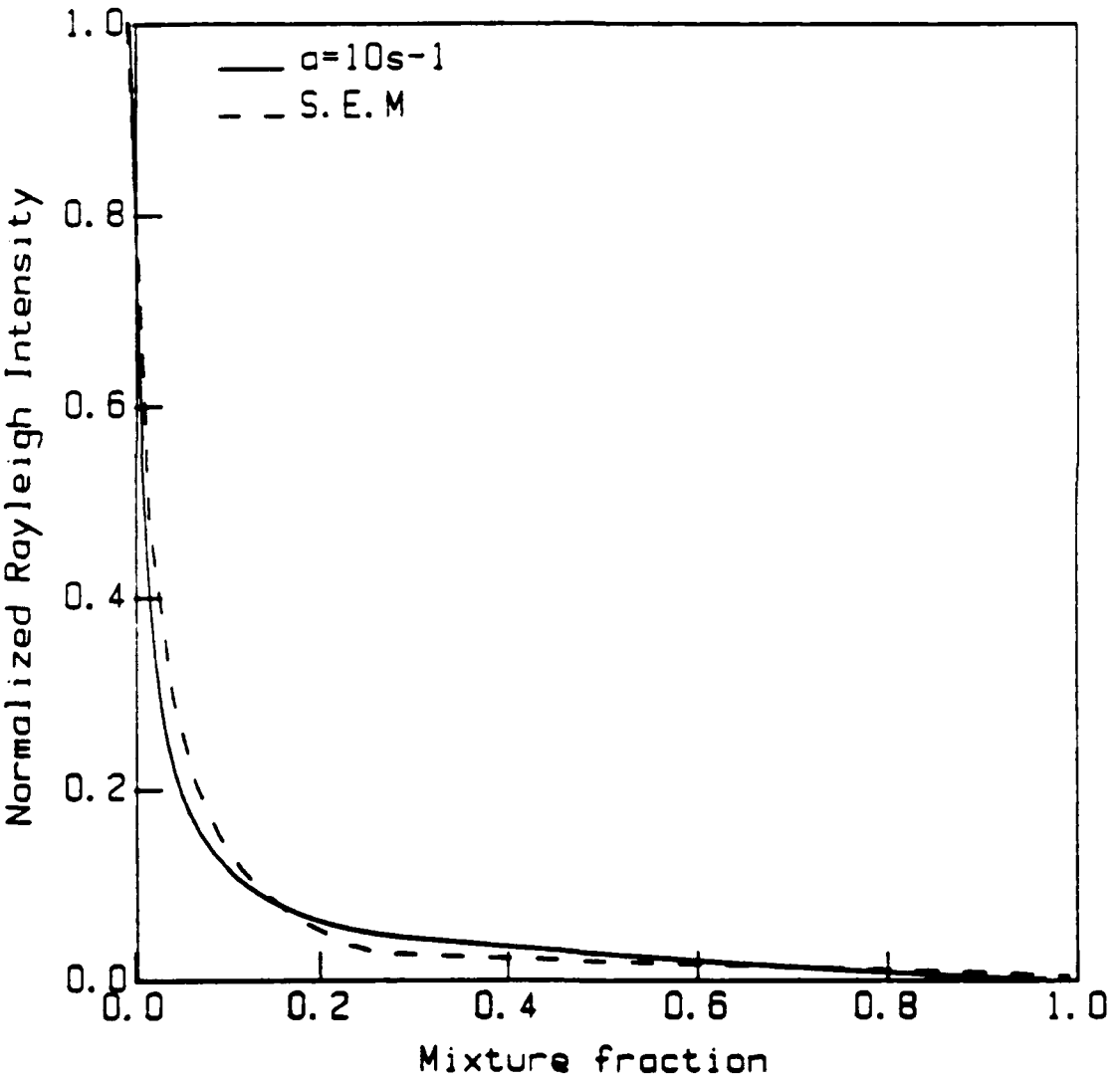
a=10s-1
S.E.M
Normalized Rayleigh Intensity
1.0
0.8
0.6
0.4
0.2
0.0
0.0
0.2
0.4
0.6
0.8
1.0
Mixture fraction

Figure 11

FLAME HOLDING IN UNCONFINED TURBULENT PREMIXED FLAMES[1]

I.G. Shepherd

Lawrence Berkeley Laboratory,
University of California,
Berkeley, CA 94720

J. R. Hertzberg and L. Talbot

Department of Mechanical Engineering,
University of California,
Berkeley, CA 94720

ABSTRACT

Detailed scalar and velocity measurements have been made in the near wake region of bluff body stabilized, lean, premixed ethylene/air flames at a cold flow Reynolds number of 3800. Two cases were studied at equivalence ratios, $\phi = 0.63$ and $\phi = 0.54$ (close to the lean blow-off limit). Transverse velocity spectra and velocity fluctuation patterns characteristic of vortex shedding were observed behind the rectangular flame holder (3 *mm* by 6 *mm*). The recirculation zone for the leaner, less stable, flame is longer (65 *mm*) than the richer case (15 *mm*) contrary to common scaling assumptions. This is probably due to the energetic, low frequency (< 70 *Hz*), irregular shedding found in the near wake of the leaner flame which may be an indicator of impending blow-off.

1. Introduction

The anchoring of premixed flames by bluff bodies has found

[1]This work was supported by the AFOSR under grant no. 84-0124. One of the authors (IGS) acknowledges the support of DOE under contract no. DE-AC-03-76SF00098.

important applications in the stabilizing of high speed combustion in ramjets and turbojet afterburners. It has also been suggested as a possible mode of flame holding in supersonic combustion devices. The flame holder region in a supersonic combustor is likely to be subsonic but whether currently available models and correlations are applicable in this regime is not known. Furthermore, in order to develop flexible numerical modeling strategies more detailed information concerning the structure of the stabilization region is essential.

Much of the early experimental work on flame stabilization was parametric in nature and directed towards the determination of blow-off limits. A variety of intuitive physical models were introduced to correlate the experimental data. Zukoski and Marble (1956), for example, made use of a Damkohler number in an ignition delay model where the critical approach flow velocity at blow-off is reached when the ignition time of the reactant mixture exceeds the time taken for a fluid element to flow past the recirculation zone. Others have treated the recirculation zone as a well stirred reactor (Nicholson and Field, 1949) or compared nondimensional heat transfer and chemical reaction rates (Spalding, 1957). These studies were broadly successful in generating reasonably robust correlations but provided only limited insight into the detailed structure of the recirculation zone and the mechanism of flame stabilization. The most significant constraint on this work was the range of diagnostic techniques available which were restricted largely to Schlieren and simple scalar measurements. More recent investigations (Fuji and Eguchi, 1981) using point measurement techniques present a more complete picture but the character of the flow in the recirculation and flame stabilization region is still unclear. There is little evidence, for example, of vortex shedding in bluff body stabilized flames although the Reynolds number generally found in hot wakes corresponds to the vortex street regime. Cantwell and Coles (1983), for instance, have observed vortex streets in isothermal flows at Reynolds numbers upto 10^6.

In this paper the results of a detailed experimental study of unconfined premixed turbulent flame stabilization by bluff bodies are reviewed and discussed. Three cases are investigated: (a) a 'well' stabilized, lean flame, (b) a flame close to the lean blow-off limit and, for purposes of comparison, (c) an isothermal flow. The results include two-component velocity data measured by laser Doppler anemometry (LDA), gas density by Rayleigh scattering and reaction intensity by an ionization probe.

2. Experimental details

A schematic of the burner configuration is presented in figure 1. A vertical jet, 51 *mm* in diameter, of premixed ethylene/air is surrounded by a co-flowing, co-axial air jet which shields the reactant stream from interaction with the ambient air. The flow is unconfined and no acoustic resonances are observed in the approach flow spectrum. 5% isotropic turbulence of integral length scale 2 *mm*, is generated by a square grid of 1 *mm* cylindrical rods with 5 *mm* spacing placed 50 *mm* upstream of the nozzle exit. The flame holder, a bar of 6.4 *mm* by 3.2 *mm* cross section, is placed 75 *mm* downstream of the nozzle exit transverse to the mean flow direction. Coordinate directions, measured from the top center of the flame holder, are Z in the axial direction (U velocity) and X in the transverse direction (V velocity).

Flame holding at two equivalence ratios was investigated: a very lean flame, close to lean blow-off at equivalence ratio $\phi = 0.54$ and a richer flame, $\phi = 0.63$, the 'well' stabilized case. The Damkohler numbers for both of the flames are much greater than unity indicating that the flame brush away from the stabilization region may be characterized as a wrinkled laminar flame zone. Isothermal measurements were also made and experimental conditions are referred to by subscripts l, r and i for the lean, richer and isothermal cases respectively. The freestream velocity is 6 m/s in all cases which gives a cold flow Reynolds number of 3800 based on the wake width (defined as the distance between u_{rms} peaks).

A two-color LDA system was used to measure the axial and transverse velocity components and, as both the components undergo flow reversal in the recirculation zone behind the flame stabilizer, all the beams were frequency shifted to give a $12 m/s$ offset. Velocity bias effects were corrected by weighting the data by the time between signal validations. Mean and rms velocities were calculated from 8192 data and spectra of the transverse velocity component were obtained by sampling the analog signal at 5 kHz.

Point determinations of the gas density were obtained by Rayleigh scattering with a probe volume of 0.1 *mm* x 0.1 *mm*. The variation in scattering cross-section across the flame front is approximately 5% in lean ethylene/air flames and so the Rayleigh intensity data can be directly interpreted as gas density. Mean density statistics and scalar spectra were calculated.

The total ion concentration across the flame brush which is a measure of the reaction intensity is determined by an uncooled double Langmuir-type probe with an active length of 5 mm.

3. Results and Discussion

3.1. Mean velocity field

Figure 2 a,b show the right hand side of the mean velocity fields for the two flame cases. In these figures the magnitude of the vectors may be best appreciated if it is recalled that the velocity in the freestream is 6 m/s. Also marked on the figures are the mean positions of the turbulent flame zone which are derived from Rayleigh scattering data. The most immediately observable difference between the two cases is the length of the recirculation zone, L. For the leaner case $L_l = 65\ mm$ which is twice as long as the richer case, $L_r = 32\ mm$, indicating that, near lean blow-off, this length is not a good indicator of flame stability. L_l and L_r are both longer than the isothermal case which is in agreement with other studies (Chen et al, 1988).

The point at which the flame can be considered fully ignited can be deduced from the position of the flame zone relative to the shear layer between the freestream and the recirculation zone. In the richer case the flame is able to propagate out of the shear layer at $0.5L_r$ but in the lean case this takes place downstream of the rear stagnation point and so the convection times to self propagation differ by a factor of five. The chemical times, estimated from the laminar flame thickness and laminar burning velocity, however, differ by a factor of three indicating that problems may be encountered if stability criteria are based on comparisons of these times. The establishment of a propagating flame is also observable in the affect of the flame on the mean velocity vectors. Downstream of the recirculation zone and away from the wake region the velocity vectors are deflected towards the centerline as the reactants are burned, expand and so are accelerated at the flame front. Since the included angles for the flames are small ($\theta_l = 7^\circ$, $\theta_r = 16^\circ$) this acceleration is primarily in the transverse direction. Where the flame is in the shear layer, however, and not fully established little of no deflection occurs: this is clearly seen in the leaner case. It may also be noted that the growth of in the flame brush thickness, δ_T, is small in the leaner case indicating

little interaction with the freestream turbulence which, in a freely propagating flame, causes the flame brush to grow by turbulent diffusion (Goix et al, 1989) as can be seen in the richer case. There is an increase of 25% in $(\delta_T)_l$ between $Z = 20$ *mm* and $Z = 40$ *mm* while over the same distance $(\delta_T)_r$ increases by a factor of 3.

3.2. Velocity Fluctuations and Spectra

Velocity measurements made at the nozzle exit show that the turbulence structure is isotropic and has an energy spectrum characteristic of grid turbulence. The structure of the recirculation zone in isothermal conditions will be analysed briefly as it will aid in the interpretation of the velocity fields of the combusting cases. The cold flow Reynolds number of 3800 indicates that vortex shedding behind the bar is to be expected and the transverse velocity spectrum has a prominent, narrow peak at 100 Hz. The Strouhal number of 0.16 is lower than that observed for cylindrical bluff bodies (0.2) but this may be expected due to the rectangular shape of the bar. The energy of the peak in the spectra has a maximum at the end of the recirculation zone, $Z = 25$ *mm*, and thereafter decays slowly. The vortex shedding also has a marked effect on the distribution of the velocity fluctuations and figures 3 a,b show contour maps of the axial and transverse velocity fluctuations for the isothermal case. The maximum axial fluctuations, figure 3 a, are found in the shear layer between the recirculation zone and the freestream. The maximum transverse fluctuations, figure 3 b, however, occur at the centerline and are due to the alternately shed vortices being swept across the centerline. These phenomena are characteristic of vortex shedding behind bluff bodies (Cantwell and Coles, 1983) and the results are summarized in Table I where L is the recirculation zone length and f the shedding frequency.

Table I: Recirculation Zone Data					
ϕ	Re	L mm	f Hz	u_{max} m/s	v_{max} m/s
0.0	3800	27	100	1.94	2.23
0.54	150	65	70	1.78	1.00
0.63	110	32	80	1.00	0.64

Figures 4 a,b and 5 a,b compare the axial and transverse velocity fluctuation contour plots for the two flame cases. The center of the flame brush is also marked on these figures. In considering these results it is important to distinguish the various causes of velocity fluctuations above those found in the freestream (approximately 0.2 m/s). In regions where the instantaneous flame front is flapping across the measurement point the velocity difference between the burnt and unburnt gases will produce an apparent increase in the velocity fluctuations (Cheng, 1984). As mentioned above, this acceleration occurs predominately in the transverse direction and its effect can be seen most clearly in the v_{rms} contour plot for the richer case, figure 4 b, where significant fluctuations along the mean flame position start to appear as the flame separates from the shear layer at $Z = 15\ mm$. Axial fluctuations in the richer case, figure 4 a, only increase in the flame zone where the mean flame angle has changed sufficiently for the acceleration to contribute to the axial velocity component. The leaner flame, figures 5 a,b, is markedly different and the presence of the flame has little effect on the velocity fluctuations in either component. This underlines the largely passive nature of the flame during the initial phase of its development.

The other major region of velocity fluctuation increase in both the combusting cases is the recirculation zone. The maximum velocity fluctuations in the recirculation zone are given in Table I. The maxima are somewhat reduced from the isothermal values and this is probably due to the volumetric expansion and the much reduced Reynolds number. Setting aside those factors associated with the flame zone which were considered above, it is clear that the distributions of velocity fluctuations are very similar to

the isothermal case. The position of the peak velocity fluctuations and its evolution occur with the same pattern and indicate the existence of vortex shedding in the near wake region. Figure 6 shows the transverse velocity spectra on the centerline for the two flames at $Z = 20\ mm$. The spectrum of the richer flame at the centerline at $Z = 20\ mm$ has a sharp, energetic peak at 80 Hz which gives a Strouhal number of 0.1. An isothermal value (Okajima, 1982) for square cylinders of 0.13 has been measured but estimation of the Reynolds number in the wake is not straightforward. The bluff body is not in uniform flow but, using the kinematic viscosity in the hot wake, the width of the flame holder and the freestream velocity, a value of 110 is obtained. These results, with the distribution of the velocity fluctuations, indicate the existence of vortex shedding behind the flame holder. The spectrum of the leaner flame, which has a slightly higher Reynolds number of 150, has a small peak at 70 Hz. The main feature of the spectrum, however, is the large amount of energy below the shedding frequency which shows that the shedding has become highly irregular. This may explain the large size of the recirculation zone and may be viewed as a precursor to blow-off. It is of interest to compare the spectrum of the density fluctuations at the same height above the flame holder but at the center of the flame brush, figure 7. The large velocity fluctuations do not strongly affect the flame oscillations and so a measurement technique such as Schlieren, which detects density gradients, would not reveal the unsteady nature of the recirculation zone.

3.3. Scalar measurements

The Rayleigh measurements have been used to delineate the xtent of the flame zone and to derive spectra of density fluctuations. Further insight into the development of the flames may be obtained from a consideration of the probability density functions (pdf) of the Rayleigh scattering intensity. Figure 8 a,b shows the density pdfs at the center of the flame brush for the two flames from $Z = 5\ mm$ to $Z = 50\ mm$. When the flame brush is large compared to the laminar flame thickness, ie in the wrinkled laminar flame regime, the pdf will be strongly bimodal with a low probability of detecting densities other than those characteristic of the burned or unburned gases. This can be clearly seen for positions $Z > 15\ mm$ of the richer case when the flame has propagated out of the shear layer. The leaner flame remains largely

within the shear layer, the bimodality is much less apparent, and close to the flame holder a broad distribution of densities is observable. At this position $(\delta_T)_l = 1.5\ mm$ which is of the same order as the laminar flame thickness ($0.8\ mm$) and therefore this distribution could arise from a weakly fluctuating laminar flame. The ion probe results, figure 9, show that this is not the case and that very little chemical reaction is taking place at these positions. It is of interest to note that the integrated ion current, in the richer case, rises to a maximum at the point where the flame leaves the shear layer.

4. Conclusions

The understanding of bluff body flame holding has largely been obtained by the use of dimensional reasoning based on relatively simple physical models which assume steady recirculation behind the flame stabilizer. Whether these concepts are applicable to flame anchoring in super sonic combustors is unclear.

A detailed experimental investigation of lean ethylene/air flame stabilization has been presented here as a step towards a more complete understanding of flame holding. This study shows that vortex shedding which was observed in the near wake of the flame holder can have significant affects on the flame stability. Close to the lean blow-off limit the shedding becomes highly irregular and is probably the cause of the large increase in the recirculation zone length and the higher velocity fluctuations. These phenomena may be indicators of impending blow-off and may indeed be responsible for it.

5. Acknowledgement

This work formed part of the Ph.D. thesis of Jean Hertzberg : *Stabilization of an unconfined flame by a bluff body*, University of California, Berkeley, 1986.

6. References

(1) Chen, T.H., Gross, L.P., Trump, D.D. and Schmoll, W.J. 1988, 24th Joint Propulsion Conference, 88-3194, Boston, Mass.

(2) Cheng, R.K. 1984, *Conditional sampling of turbulence intensities and Reynolds stress in premixed turbulent flames,* Combustion Science and Technology, 41, p109.

(3) Fuji, S. and Eguchi, k., 1981, *A comparison of cold and reacting flows around a bluff-body flame stabilizer,* Journal of Fluids Engineering, 103, p. 328

(4) Goix, P., Parentheon, P. and Trinite, M. 1989, *A tomographic study and Lagrangian interpretation of a V-shaped premixed flame,* Combustion and Flame, to be published.

(5) Nicholson, H.M. and Field, J.P., 1949 *Some experimental techniques for the investigation of the mechanism of flame stabilization in the wakes of bluff bodies,* 3rd. Symposium (Int.) on Combustion, p. 44

(6) Okajima, A., 1982 *Strouhal numbers of rectangular cylinders,* Journal of Fluid Mechanics, 123, p. 379

(7) Zukoski, E.E. and Marble, F.E., 1956, *Experiments concerning the mechanism of flame blow-off from bluff bodies,* Proc. Gas Dynamics Symposium on Aerothermochemistry, Northwestern University, p. 205

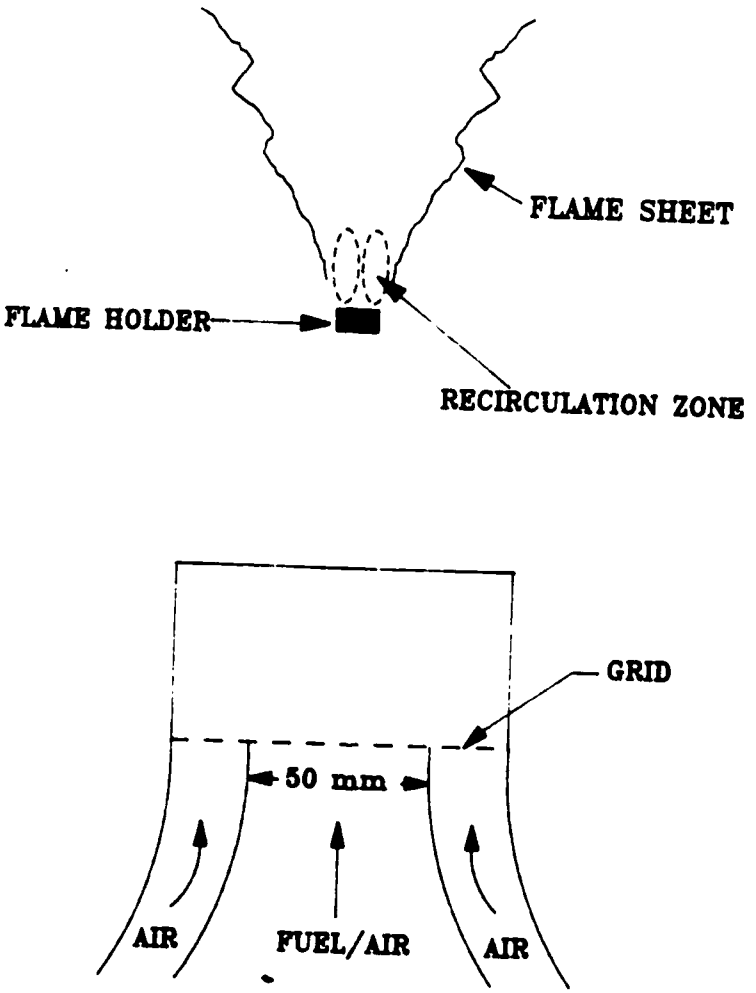

Figure 1. Burner Configuration.

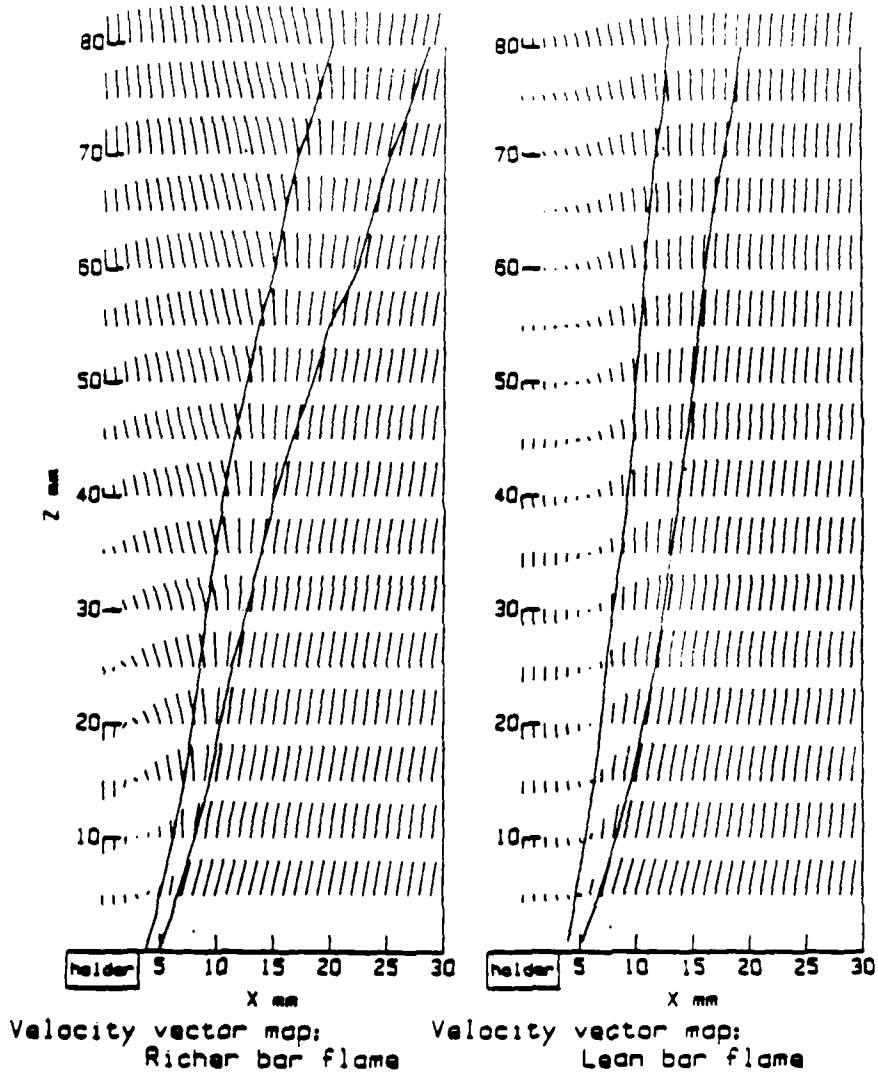

Figure 2. Mean Velocity Field.

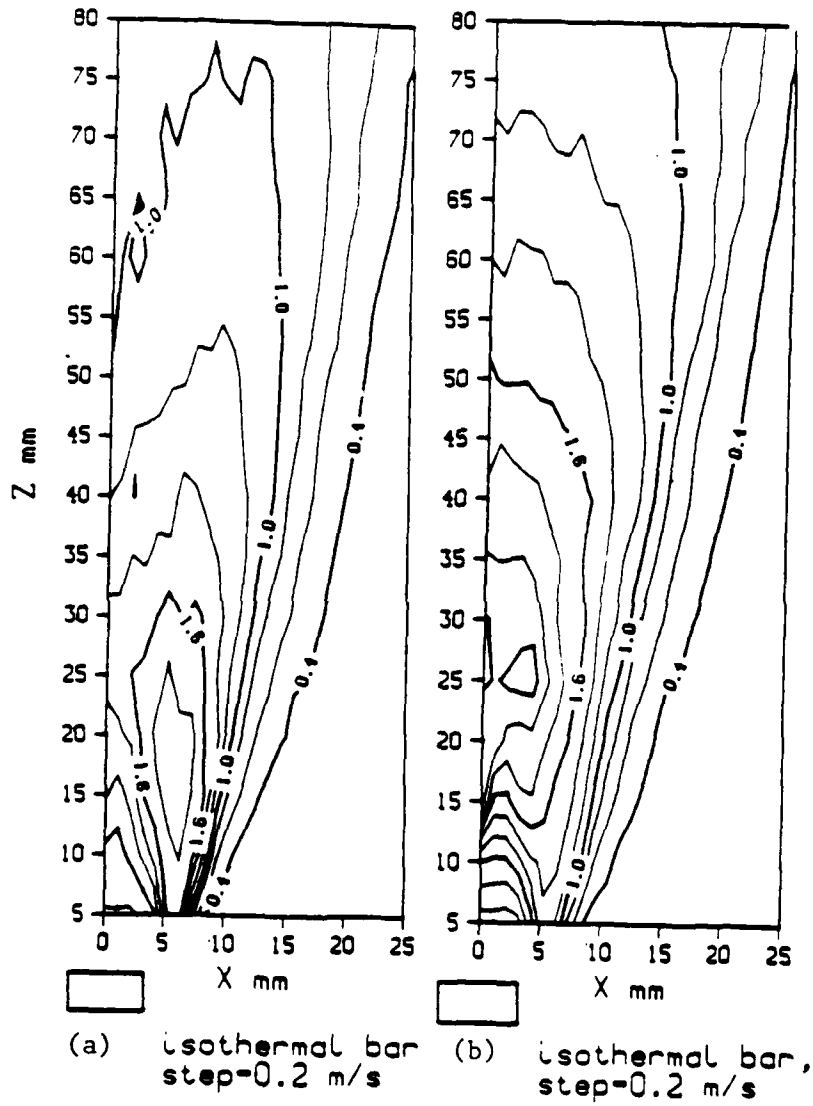

Figure 3. Velocity Fluctuations a) axial b) transverse

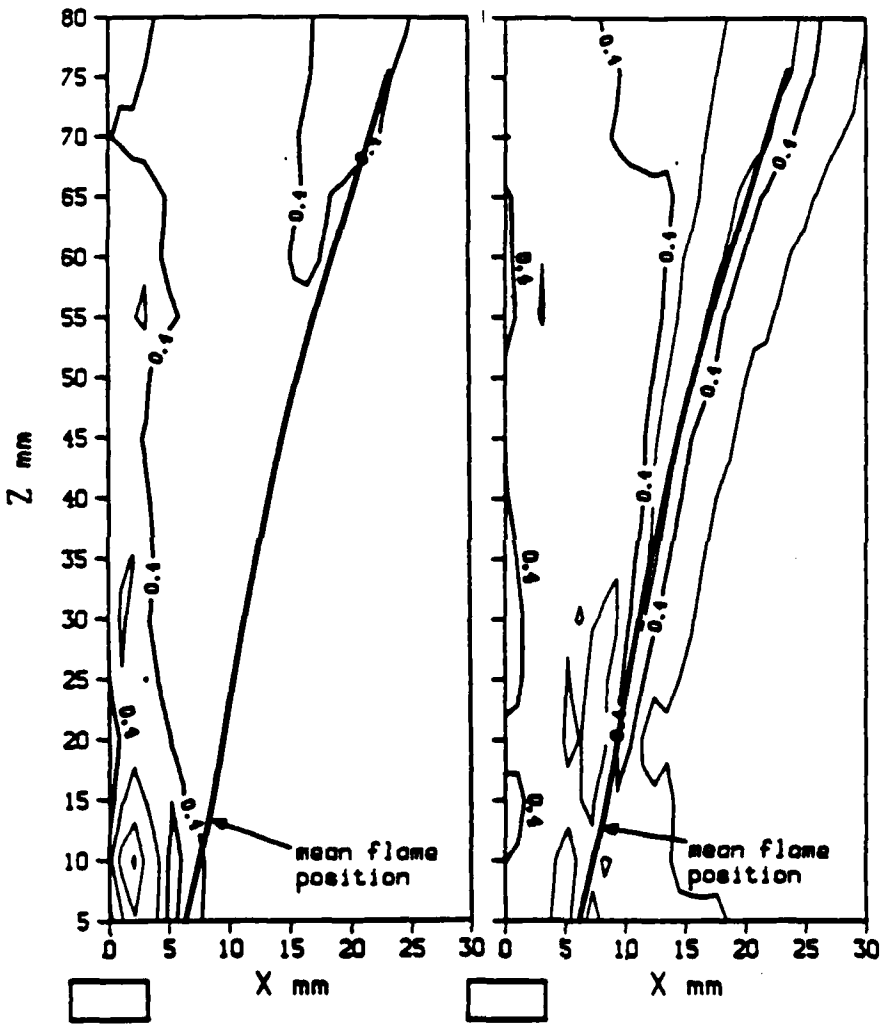

Figure 4. Velocity Fluctuations a) axial b) transverse.

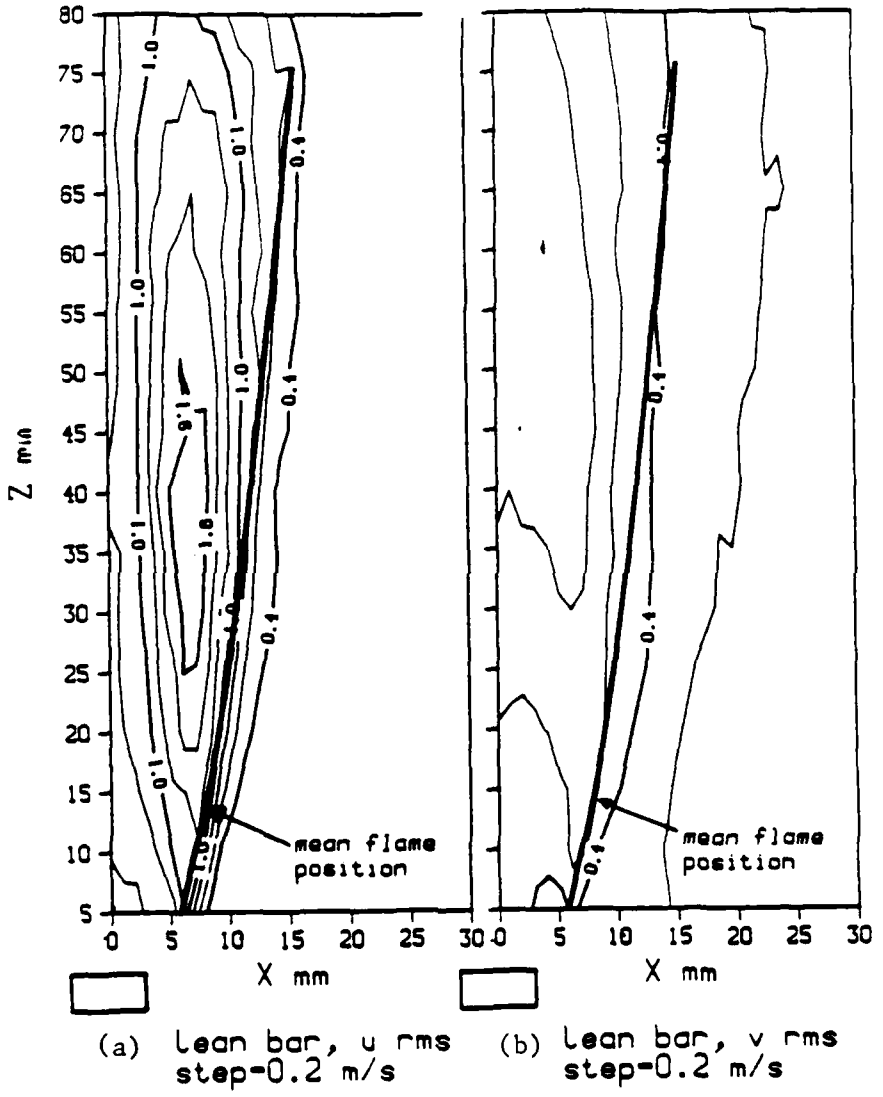

Figure 5. Velocity Flucuations a) Axial

b) transverse.

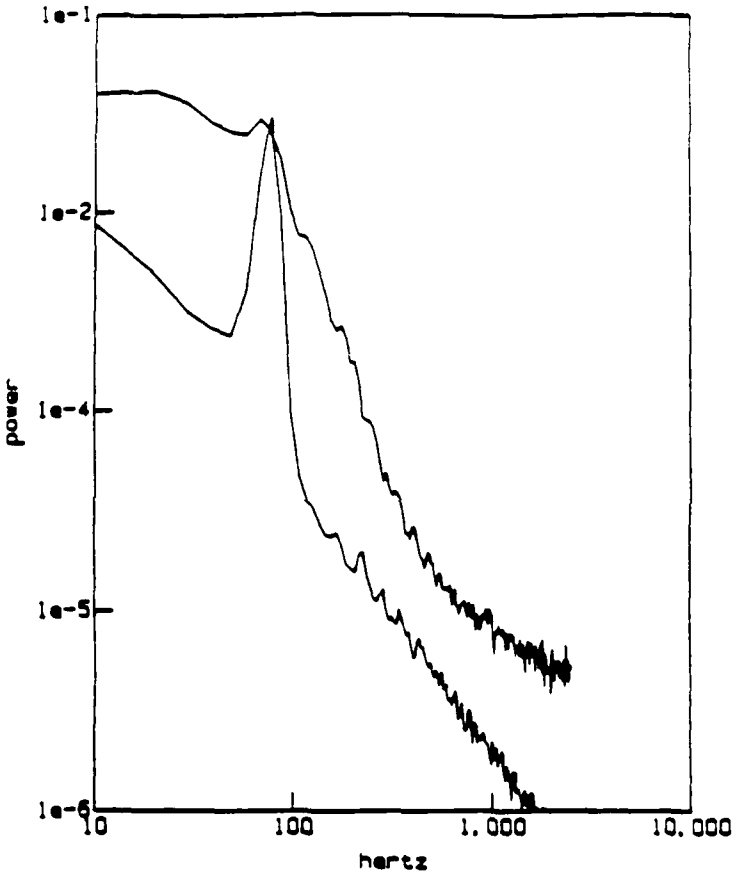

Figure 6. unscaled v velocity spectra
upper = lean bar Z=20. x=0
lower = richer bar Z=20. x=0

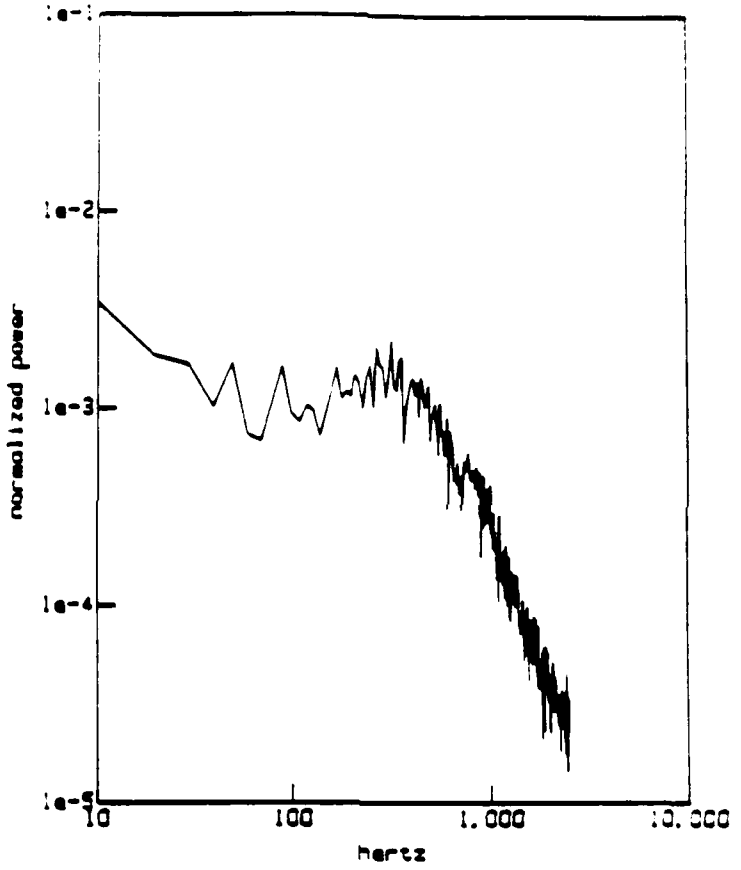

Figure 7. density spectra
lean bar flame. Z = 20 mm
center of flame

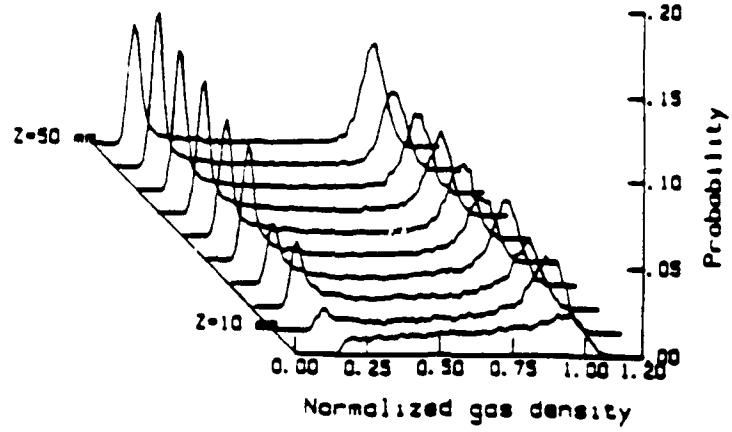

(a) PDF of density at center of flame as downstream distance increases in 5mm steps Richer bar flame

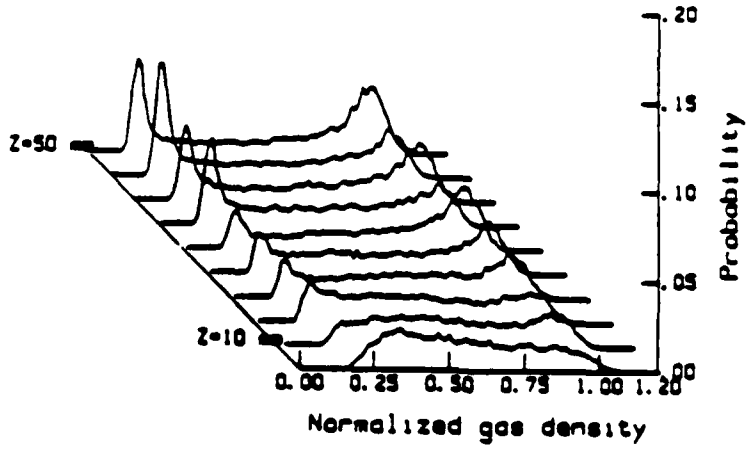

(b) PDF of density at center of flame as downstream distance increases in 5mm steps Lean bar flame

Figure 8.

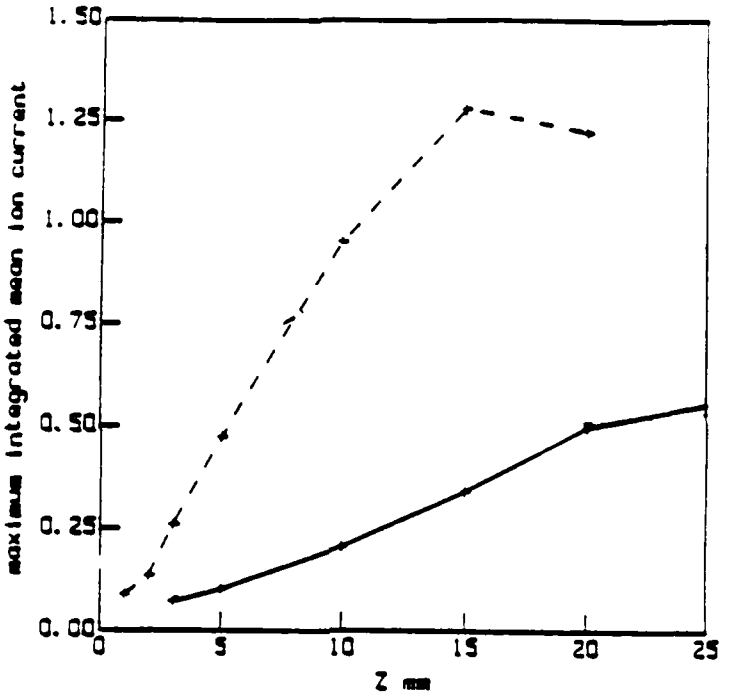

Figure 9. Max ion current vs downstream location
richer bar = dashed line
lean bar = solid

P158. **Experimental Study of Turbulent Counterflow Diffusion Flame Structure**

P.J. Goix, L. Talbot

Mechanical Engineering Department,
U.C. Berkeley, CA 94720.

ABSTRACT

A Hydrogen-Helium mixture has been chosen to investigate the dilution effects on the structure of the diffusion flame. To investigate the combustion effects on the turbulent mixing, reacting and non reacting conditions have been studied at the same Reynolds number. In order to study the reaction zone structure, high speed tomography based on Mie scattering has been employed using a copper vapor laser and a Fastax high speed camera. Different seeding techniques have been used to visualize both the turbulent air and fuel jets. The tomographic records were digitized and recorded in a digital computer for statistical treatment. Significant differences in the wrinkle scales between the reacting and the non reacting flows were found. A fractal statistical analysis of the tomography records has been done to quantify these differences. Seeding of both fuel and air jets provided a mean for the evaluation of the reaction zone thickness. From the time resolved tomographic records an evaluation of the stretch of the reaction zone boundaries has been performed. Local flame extinction and reignition have been observed for different H2/Helium fuel mixture. Further statistic on reaction zone thickness are still in progress.

P183.

Direct Measurement of Mixture Fraction in Reacting Flow Using Rayleigh Scattering

P.J. Goix, K.R. Leonard, L. Talbot and J.Y. Chen (*)

Mechanical Engineering Department,
U.C. Berkeley, CA 94720.

(*) Sandia National Laboratory CRF,
Livermore, CA 94550.

Abstract

The mixture fraction variable, ξ, is very useful in describing reaction zone structure in non-premixed flames. Extinction limits and turbulent mixing are often described as a function of this variable. Experimental evaluation of ξ is valuable in understanding the influence of turbulent mixing on the chemistry process. Historically, the evaluation of mixture fraction in combusting flow has required multiple concentration measurements. Here, a fuel has been designed to permit the measurement of the mixture fraction using only Rayleigh scattering. A Rayleigh intensity/ mixture fraction correspondence has been obtained experimentally in a laminar coflow flame. The influence of strain rate and differential diffusion effects has been investigated using a laminar counterflow diffusion flame and shifting equilibrium models. The results obtained from these comparisons are very encouraging and suggest that the Rayleigh/ mixture fraction correspondence established, is valid under both turbulent mixing and laminar strained flamelet combustion regimes.